Applied Energy 341 (2023) 121007

Contents lists available at ScienceDirect

Applied Energy

journal homepage: www.elsevier.com/locate/apenergy

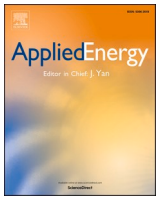

Stochastic, resilience-oriented optimal sizing of off-grid microgrids considering EV-charging demand response: An efficiency comparison of state-of-the-art metaheuristics

Soheil Mohseni [a,*], Roomana Khalid [a], Alan C. Brent [a,b]

[a] Sustainable Energy Systems, School of Engineering and Computer Science, Wellington Faculty of Engineering, Victoria University of Wellington, PO Box 600, Wellington 6140, New Zealand
[b] Department of Industrial Engineering and the Centre for Renewable and Sustainable Energy Studies, Stellenbosch University, Stellenbosch 7600, South Africa

HIGHLIGHTS

- A novel holistic method for off-grid microgrid planning optimisation is introduced.
- The potential of state-of-the-art metaheuristics in better nearing global optimality is shown.
- A high penetration of EVs are integrated using specific demand response strategies.
- The importance of energy resilience in isolated microgrid sizing is highlighted.
- The potentially significant impact of characterising uncertainties in optimal microgrid planning is substantiated.

ARTICLE INFO

Keywords:
Microgrids
Optimal sizing
Metaheuristics
Electric vehicles
Renewable energy sources
Resilience

ABSTRACT

The resilient microgrid (MG) capacity planning and optimisation problem is widely recognised as a non-deterministic polynomial time-hard (NP-hard) problem. Accordingly, metaheuristics – top-level algorithms inspired by various natural and physical processes – can be utilised to determine the near optimality in designing MGs. However, a comprehensive review of the mainstream literature has shown that the performance of several metaheuristics has not yet been evaluated. In response, this paper first systematically benchmarks the efficiencies of previously unexplored metaheuristics in MG sizing applications against the well-established metaheuristic in the literature, namely the particle swarm optimisation (PSO) algorithm. To this end, the metaheuristics are separately integrated into a novel MG sizing method, which is aware of the optimal demand response capacity procured from electric vehicle (EV)-charging loads. Two grid-independent, 100%-renewable MGs are modelled, which enable the reliable and robust supply of electrical loads in areas far removed from the grid. Furthermore, an advanced EV-charging demand response program is integrated into the overall method, whilst quantifying various sources of time-series data uncertainty and considering specific resilience constraints. The simulation results yielded from three real-world isolated community case studies in Aotearoa-New Zealand confirm the effectiveness of the proposed stochastic, resilience-oriented, EV-charging demand response-addressable MG sizing method. Importantly, the comprehensive statistics-based performance evaluations indicate that new metaheuristics have the potential to outperform the PSO by up to ~6% in MG sizing applications. This indicates the potentially significant implications of using advanced metaheuristics for improving the economics – and, therefore, rolling out – capital-intensive grid-isolated 100%-renewable MGs.

1. Introduction

The optimal designing of microgrids (MGs) has the potential to play a significant role in the best use of limited resources, particularly in view of increased transportation sector electrification interventions, variable renewables integrations, and energy resilience considerations [1–4]. A holistic perspective when designing integrated sustainable energy systems is not only effective to reduce total discounted system costs, but also enables more robust MG designs. However, such designing

* Corresponding author.
E-mail address: soheil.mohseni@ecs.vuw.ac.nz (S. Mohseni).

https://doi.org/10.1016/j.apenergy.2023.121007
Received 30 December 2022; Received in revised form 1 March 2023; Accepted 19 March 2023
Available online 21 April 2023

Nomenclature

Abbreviations

ABC	Artificial Bee Colony
ACO	Ant Colony Optimisation
AGTO	Artificial Gorilla Troops Optimiser
AHA	Artificial Hummingbird Algorithm
ALO	Ant Lion Optimiser
BBO	Blockhole-Based Optimisation
BESS	Battery Energy Storage System
BOA	Bat Optimisation Algorithm
CSA	Cuckoo Search Algorithm
DA	Dragonfly Algorithm
DE	Differential Evolution
DR	Demand Response
EO	Equilibrium Optimiser
EV	Electric Vehicle
GA	Genetic Algorithm
GOA	Grasshopper Optimisation Algorithm
GSA	Gravitational Search Algorithm
GWO	Grey Wolf Optimiser
MFOA	Moth-Flame Optimisation Algorithm
MG	Microgrid
MPA	Marine Predator Algorithm
NPC	Net Present Cost
PDF	Probability Density Function
PSO	Particle Swarm Optimisation
PV	Photovoltaic
SSA	Salp Swarm Algorithm
TNPC	Total Net Present Cost
WCA	Water Cycling Algorithm
WHO	Wild Horse Optimiser
WT	Wind Turbine

problems are associated with more mathematically complex formulations – specifically, non-deterministic polynomial time-hard (NP-hard) problems – for which no polynomial time-addressable solution exists [4–9].

In this light, the importance of metaheuristic optimisation algorithms for MG capacity planning is widely recognised [10]. More specifically, metaheuristics iteratively move the randomly initialised particles in the solution space with respect to a specifically defined metric for the fitness of re-positioned particles. Accordingly, they eliminate the need for approximating the solution space – using, for example, specifically developed decomposition methods – and, therefore, can be applied to NP-hard problems [11]. This enables metaheuristics to better determine the globally optimum solution to the problem under consideration [12].

1.1. Literature review: Knowledge gaps

In the MG designing literature, a wide variety of metaheuristics, including both single and hybrid algorithms, have been effectively utilised [10,13,14]. In view of the fact that metaheuristics are inherently approximate algorithms, they have been recognised to be associated with varied efficiencies when applied to different nonlinear, non-convex MG designing problem formulations. Accordingly, the performance of new metaheuristics needs to be continuously tested in MG designing applications in a systematic manner [15–17].

In this context, several studies have sought to conduct comparative analyses of metaheuristics. For instance, Fathi et al. [18] have recently explored the comparative efficiencies of the particle swarm optimisation (PSO), the differential evolution (DE), the grey wolf optimiser (GWO), and the water cycling algorithm (WCA) in stand-alone MG sizing applications. Bukar et al. [19] have also shown the superiority of the grasshopper optimisation algorithm (GOA) to the GWO, the dragonfly algorithm (DA), the cuckoo search algorithm (CSA), the salp swarm algorithm (SSA), and the ant lion optimiser (ALO) in solving grid-independent MG designing problems. In another instance, Sukumar et al. [20] have demonstrated the outperformance of the GWO to the PSO, the artificial bee colony (ABC), the gravitational search algorithm (GSA), and the genetic algorithm (GA) for the optimal sizing of battery energy storage systems (BESSs) integrated into MGs. Diab et al. [14] have gone further and compared the efficiencies of the equilibrium optimiser (EO), the bat optimisation algorithm (BOA), and the blackhole-based optimisation (BBO) technique, identifying the EO as the most effective algorithm. Abo-Elyousr et al. [21] have, additionally, analysed the efficiency improvement of the PSO when hybridised with the ant colony optimisation (ACO), and have shown its outperformance to the single PSO and ACO in non-grid-connected MG sizing applications.

As the above review of the studies focused on the comparative analyses of different metaheuristics in designing various MG configurations indicates, there exists a glaring inconsistency in the ranking of metaheuristics in MG capacity planning applications. Such inconsistencies can be explained by a combination of: (i) the absence of statistical tests (and hence statistical criteria) in the associated efficiency comparisons, and (ii) the lack of attention to the fact that the performance of metaheuristics could vary considerably in different MG sizing problem settings, particularly in terms of system configuration and the underlying load and meteorological data. This indicates that a systematic, multi-case-oriented, summary statistics-based approach is needed to generate more robust generalisations of the effectiveness and utility of metaheuristics against each other.

On the other hand, a major driver for deploying MGs is their ability to provide resilience benefits [22–26]. Accordingly, the grid-connected MG sizing literature has widely explored the relative importance of different resilience preferences on the MG sizing decision-making processes. For instance, Marqusee et al. [27] have investigated the on-grid MG sizing problem in the presence of a specifically defined energy resilience constraint that probabilistically quantifies the amount of time it can sustain loads when the grid is out. Similarly, Masrur et al. [28] have adopted the concept of the probability of surviving outages and providing reliable power when the grid is down. In another notable instance, Anderson et al. [29] have defined outage survivability as the probability that a site can supply reliable power to critical loads for a specified outage duration. In a fundamentally different study, Wang et al. [30] have developed a resilience-driven approach for the optimal sizing and pre-positioning of mobile energy storage systems in decentralised networked MGs, where the concept of resilience is defined based on both man-made events and natural disasters.

Table 1 provides a synopsis of the salient previous work on the long-term strategic investment planning optimisation of renewable and sustainable energy systems considering uncertainties and flexible load programmes. A more comprehensive version of the table is provided as Supplementary Material accompanying the paper (Additional File 1: Overview of the previous work on stochastic, DR-addressable MG sizing).

A comprehensive review of previous work on the optimal MG sizing has identified that grid-connected MG sizing studies have increasingly factored in resilience constraints during the long-term strategic investment planning phases. However, the wider approaches in the mainstream off-grid MG sizing literature generally lack coordinated resilience constraints, despite the arguably greater importance of the

Table 1
Overview of the studies on the long-term strategic optimal sizing of renewable and sustainable energy systems.

Ref.	Technologies in the candidate pool	DSM strategy	Responsive load sector(s)	Uncertainty treatment technique	Parametric uncertainty sources	Optimisation algorithm	Geographical scope
[31]	Wind, non-renewables, main grid	ICSs	Residential	MCS	Renewable generation, load	GA	Town
[32]	Unspecified renewables, main grid	ICSs	Unspecified	PEM	Load demand	SP	Region
[33]	Wind, BESS, main grid	RTP	Residential	MCS	Renewable generation, load, wholesale prices	PSO	Building
[34]	Solar PV, solar thermal, BESS, non-renewables, main grid	DLC	E-mobility	MCS	Load demand	MILP	Neighbour-hood
[35]	Wind, BESS, non-renewables, main grid	ToU	Residential	MCS	Renewable generation, load	MIP	Rural community
[36]	Wind, solar PV, PHS	ToU	Unspecified	MCS	Renewable generation	PSO	Region
[37]	Wind, solar PV, BESS, non-renewables, main grid	RTP	Residential	MCS	Renewable generation, load	MILP	Building
[38]	Wind, solar PV, BESS	RTP-ICSs	Residential	MCS	Renewable generation	MILP	Remote community
[39]	Solar PV, CHP, BESS, TS, main grid	RTP-ICSs	Unspecified	MCS	Renewable generation, load, wholesale prices	NSGA-II	City
[40]	Solar PV, CHP, boiler, BESS, main grid	ToU	Unspecified	MCS	Renewable generation, load	MINLP	Neighbour-hood
[41]	Wind, CHP, boiler, BESS, TS, main grid	ToU	Unspecified	MCS	Renewable generation, load	MINLP	Neighbour-hood
[42]	Wind, solar PV, BESS, TS, non-renewables, main grid	ICSs	Residential	Interval analysis	Renewable generation, load	NSGA-II	Town
[43]	Wind, CHP, main grid	RTP	Industrial, residential, commercial	MCS	Renewable generation, load	SP	Town

Key: BESS = Battery Energy Storage System, CHP = Combined Heat and Power, DLC = Direct Load Control, DSM = Demand-Side Management, GA = Genetic Algorithm, ICSs = Interruptible/Curtailable Services, MCS = Monte Carlo Simulation, MILP = Mixed-Integer Linear Programming, MINLP = Mixed-Integer Nonlinear Programming, MIP = Mixed-Integer Programming, NSGA-II = Non-dominated Sorting Genetic Algorithm II, PEM = Point Estimate Method, PSO = Particle Swarm Optimisation, PV = Photovoltaic, RTP = Real-Time Pricing, SP = Stochastic Programming, ToU = Time-of-Use, TS = Thermal Storage.

concept of energy resilience in isolated communities. This indicates that designing stand-alone MGs using existing methods, especially in 100%-renewable configurations, fails to adequately capture the true value the target communities place on the security of supply. Accordingly, a new grid-isolated MG design optimisation modelling framework that incorporates some heuristic constraints for resilience is needed to facilitate site-specific decisions on the trade-offs between cost and resilience. It is also noteworthy that given the recent advances in adapting wind turbines (WTs) to extreme weather conditions, particularly the introduction of 'survival mode' for WTs, the extreme weather event impacts on solar photovoltaic (PV) systems are increasingly considered to be comparatively more important and pronounced [44,45].

Moreover, a recent growing body of literature has effectively shown that MGs can play a significant role in enabling the electrification of transportation at scale by providing flexibility provisions [46–50]. For example, Haupt et al. [51] have comprehensively studied the relative impact of a variety of electric vehicle (EV) charging strategies on the sizing of BESSs in charging hub MGs. Mortaz et al. [52] have presented an optimisation model for siting and sizing of vehicle-to-grid facilities in grid-tied MGs, whilst characterising the associated parametric sources of uncertainty. Furthermore, Harsh and Das [53] have formalised an optimal demand response (DR) coordination strategy based on EV-charging flexibility resources for the energy management of reconfigurable grid-connected MGs.

Whilst considerable effort has been devoted to analysing the impact of tailor-made dispatch strategies for the optimal system integration of EV-charging loads in grid-connected MGs, less attention has been given to specifically developed scheduling strategies for grid-isolated systems. This is despite the common knowledge that the positive impact of effective peak shaving and load levelling strategies is more striking in the absence of a utility grid – due to the substantial reduction of the over-capacity needed in a fully renewable stand-alone MG. Accordingly, a truly optimal off-grid MG planning approach that is able to effectively serve EV-charging loads is needed.

1.2. Novel contributions

To address the aforementioned knowledge gaps, this paper introduces a novel EV-charging-load-addressable MG capacity planning optimisation approach with specifically imposed resilience constraints. It then uses the developed optimisation modelling framework to systematically test the efficiencies of six competitively selected state-of-the-art metaheuristics in isolated MG applications, whilst additionally benchmarking them against the most commonly used metaheuristic in the literature, namely the PSO algorithm. More specifically, the novel contributions of the paper are as follows:

- Presenting a multi-criteria framework for the efficiency comparison of metaheuristics based on descriptive statistics and the results obtained from various test cases to systematically account for the robustness in achieving the optimal solution and the convergence rate.
- Evaluating the efficiency of a number of previously unexplored metaheuristics in MG capacity planning optimisation applications, namely: the wild horse optimiser (WHO), the artificial hummingbird algorithm (AHA), the artificial gorilla troops optimiser (AGTO), the marine predator algorithm (MPA), the equilibrium optimiser (EO), and the moth-flame optimisation algorithm (MFOA).
- Quantifying the relative importance of different levels of resilience to extreme weather events affecting the MG components on the configuration and cost of off-grid MGs. To this end, a specific sensitivity analysis is performed to approximate the possible range of the impact of resilience preferences on different off-grid MG design solutions.
- Developing a new DR-integrated rule-based energy despatch algorithm that efficiently addresses the supplying of EV-charging loads based on load factor improvement.
- Characterising various sources of parametric uncertainty in an integrated manner to appropriately reflect the underlying correlations

of the uncertainty factors, thereby preserving the associated multivariate relationships.

1.3. Organisation of paper

The remainder of this paper is organised as follows. Section 2 presents the test-case MGs conceptualised, which are employed to parametrise the proposed method, before formulating the proposed resilience-constrained off-grid MG sizing modelling framework considering large-scale electrification of the transport sector. Section 3 populates the model and test cases for the remote study areas and communities of interest, while Section 4 presents and discusses the results, including a discussion of the comparative performance of the selected metaheuristics. Finally, conclusions are drawn and prospects for further work are highlighted in Section 5.

2. Methodology

This section presents the proposed general stochastic, DR-integrated off-grid MG sizing method, which is parametrised for two 100%-renewable test-case systems conceptualised in Section 2.1. To this end, first, the underlying resilience-oriented, DR-aware, deterministic problem is formulated based on the net present valuation concept, which is then advanced to a stochastic version where the problem-inherent uncertainties are systematically quantified in a computationally efficient manner. The proposed method also provides a platform for evaluating the comparative efficiencies of the selected metaheuristics and determining their rank orders based on multi-test-case-led statistical analyses.

2.1. Test-case microgrids

Two mainstream 100%-renewable off-grid MG configurations were considered as test cases, which integrate the following generation and storage technologies: (i) solar PV, WT, and BESS, and (ii) solar PV and BESS. On the consumption side, both residential loads and EV-charging loads (integrated based on level-1 chargers) were considered. The reader is referred to the Supplementary Material accompanying the paper (Additional File 2: Case study background information and time-series data) on how the residential/commercial and EV-charging load profiles were derived. Fig. 1 depicts the schematic diagram and directions of energy flow within the two notional MGs modelled. Also, the mathematical models of the components of the MGs are presented in Appendix A.

The selection of the PV/WT/battery and PV/battery energy configurations in this study was based on the results of pre-feasibility site assessments that evaluated the potentials of various renewable energy sources in the site of interest. The assessments indicated that solar and wind energy were the most viable renewable energy sources for the specific context of a local MG that serves the targeted community with a high penetration of EVs. The assessments considered factors such as the availability of solar and wind resources, the local climate, and the site's topography. Based on these assessments, the PV/WT/battery and PV/battery configurations were identified as the most suitable for meeting the energy demands of the specific community of interest.

2.2. Objective function

The objective function of the underlying problem is to minimise the total discounted system cost. To this end, the net present cost (NPC) metric is utilised to estimate the discounted cost of each component over the project lifetime. The NPC of each component can be expressed as [54–56]:

$$NPC_c = N_c \times \left(CC_c + RC_c \times SPPW + \frac{O\&M_c}{CRF(ir, PL)} - SV_c \right). \tag{1}$$

In Eq. (1), N_c represents the optimal size of component $c \in C = \{PV, WT, Bat, Inv\}$. More specifically, it represents the optimal number of component modules for discrete decision variables including solar PV panels and WTs, as well as the optimal capacity of components for continuous decision variables including the battery bank and inverter. Also, CC_c, RC_c, and $O\&M_c$ respectively denote the capital cost, replacement cost, and operation and maintenance cost of component c. Furthermore, $SPPW$, CRF, and SV respectively denote the single-payment-present-worth factor, the capital recovery factor, and the salvage value, which can be calculated as follows [56]:

$$SPPW = \sum_{n=1}^{N} \frac{1}{(1+ir)^{CL \times n}}, \tag{2}$$

$$N = \begin{cases} \left\lfloor \frac{PL}{CL} \right\rfloor - 1, & if\ PL\ mod\ CL = 0 \\ \left\lfloor \frac{PL}{CL} \right\rfloor, & otherwise \end{cases} \tag{3}$$

$$CRF(ir, PL) = \frac{ir(1+ir)^{PL}}{(1+ir)^{PL} - 1}, \tag{4}$$

$$SV = RC \times \frac{CL - (PL - CL \times \lfloor \frac{PL}{CL} \rfloor)}{CL}, \tag{5}$$

where ir is the interest rate, PL is the project lifetime, and CL is the component's lifetime.

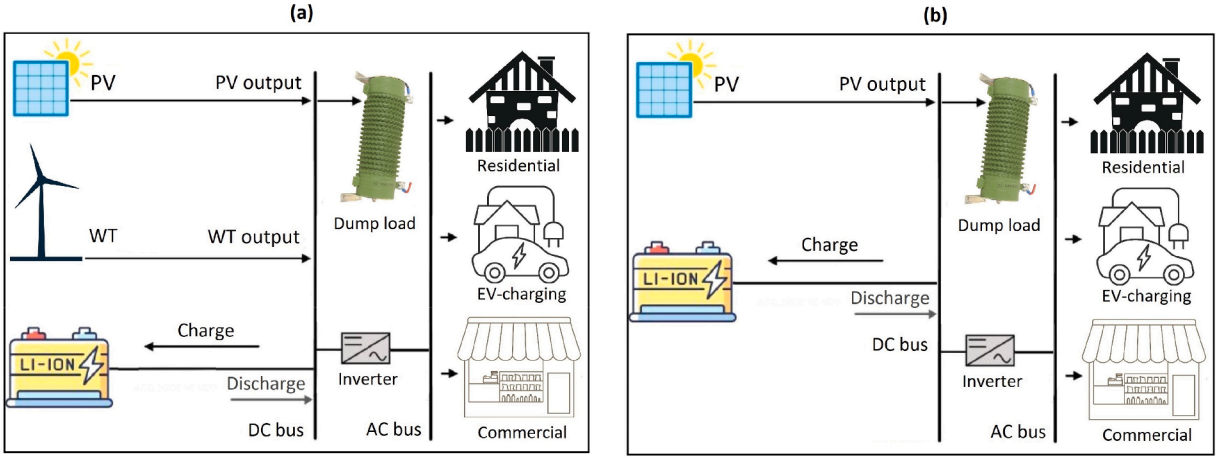

Fig. 1. Illustration of the two off-grid MG configurations: (a) PV/WT/battery, and (b) PV/battery.

Accordingly, the objective function is defined as the sum of the NPCs of the underlying components as [56]:

$$\min OF = TNPC = \sum_{c \in C} NPC_c + p, \tag{6}$$

where $TNPC$ denotes the total net present cost of the project, p is a penalty parameter that adds a sufficiently large value to the objective function when the planning-level constraints are violated, and is equal to zero in the regions of the design space where the planning-level constraints are not violated.

2.3. Constraints

The total discounted system cost is minimised subject to two interdependent sets of constraints on the dispatch and investment planning of MGs. Specifically, the operational-level constraints are applied during the energy balance analyses, whereas the planning-level constraints are, in larger part, designed to capture the preferences of decision-makers around the higher-level system performance criteria, such as reliability and resilience, and in lesser part, to help maintain the balance of analysis.

2.3.1. Operational-level constraints

The following set of operational-level constraints are active during the energy management (dispatch) phase [57–59]:

$$P_{PV}(t) + P_{WT}(t) + P_{dch}(t) + \frac{Q_L(t)}{\eta_I} + \frac{Q_{EV}(t)}{\eta_{EV}} = P_{ch}(t) + \frac{P_L(t)}{\eta_I} + \frac{P_{EV}(t)}{\eta_{EV}}, \quad \forall t \tag{7}$$

$$P_{ch}^{min} \le P_{ch}(t) \le P_{ch}^{max}, \quad \forall t \tag{8}$$

$$P_{dch}^{min} \le P_{dch}(t) \le P_{dch}^{max}, \forall t \tag{9}$$

$$E_b^{min} \le E_b(t) \le E_b^{max}, \forall t \tag{10}$$

$$E_b^{min} = (1 - DOD^{max}) \times E_b^{max}, \tag{11}$$

$$P_{ch}(t) \times P_{dch}(t) = 0, \quad \forall t \tag{12}$$

where $P_{PV}(t)$ and $P_{WT}(t)$ respectively denote the power output from the solar PV and WT generation systems at time-step t of the hourly-basis, year-long operation of the system, P_{ch} and P_{dch} respectively denote the charging power and discharging power of the stationary battery bank, P_L and P_{EV} respectively denote the residential/commercial load demand and EV-charging load, Q_L and Q_{EV} respectively denote the unserved residential/commercial load and unserved EV-charging load, η_I and η_{EV} respectively denote the efficiencies of the residential/commercial load inverter and the EV-charging load inverter, E_b is the energy content of the battery bank, DOD^{max} is the maximum depth of discharge of the battery bank, while the superscripts *min* and *max* respectively represent the minimum and maximum possible values of the corresponding variables.

The linear equality constraint in Eq. (7) ensures the MG-wide balance of power at each time-step of the system operation, while the constraints in Eqs. (8)-(11) enforce the dispatch of the battery bank to comply with the physical limits of battery storage; specifically, the associated charge and discharge power capacities and the allowable energy content range. Furthermore, the nonlinear equality constraint in Eq. (12) guarantees that the charge and discharge events of the battery storage do not occur simultaneously.

2.3.2. Planning-level constraints

The constraints that are active during the planning stage can be broadly classified into those seeking to reflect the value of energy not supplied and those aiming to accommodate more realistic approximations of reality. In this context, the constraints in Eqs. (13)-(16) model the reliability of power supply [60], while the constraints in Eqs. (17) and (18) model the battery autonomy days as a resilience metric, which is defined as the number of days the battery bank can sustain the entire load on the MG [19].

$$LPSP_L \ge LPSP_L^{min}, \tag{13}$$

$$LPSP_{EV} \ge LPSP_{EV}^{min}, \tag{14}$$

$$LPSP_L = \frac{\sum_{t=1}^{T}(Q_L(t) \times \Delta t)}{\sum_{t=1}^{T}(P_L(t) \times \Delta t)}, \tag{15}$$

$$LPSP_{EV} = \frac{\sum_{t=1}^{T}(Q_{EV}(t) \times \Delta t)}{\sum_{t=1}^{T}(P_{EV}(t) \times \Delta t)}, \tag{16}$$

where $LPSP_L$ and $LPSP_{EV}$ respectively denote the loss of power supply probabilities associated with the total residential/commercial loads and the total EV-charging loads, $LPSP_L^{min}$ and $LPSP_{EV}^{min}$ respectively denote the minimum allowable loss of power supply probabilities in supplying residential/commercial and EV-charging loads, with T denoting the number of time-steps in the year-long operation of the system, which is fixed at 8760 h.

$$AD_{bat} \ge AD_{bat}^{min}, \tag{17}$$

$$AD_{bat} = \frac{N_B C_{B,r} DOD^{max} \eta_{inv} \eta_{dch}}{\sum_{t=1}^{T}(P_L(t) \times \Delta t)}, \tag{18}$$

where the term $N_B C_{B,r}$ represents the optimal capacity of the stationary battery (as determined over the course of the iterations), AD_{bat}^{min} is the minimum allowable battery autonomy days, while the term $\sum_{t=1}^{T}(P_L(t) \times \Delta t)$ denotes the total residential/commercial loads on the MG. Recall that to minimise energy losses, the stationary battery is never discharged to serve the EV-charging loads.

Moreover, the constraint in Eq. (19) sets the initial energy in-store to the maximum possible value (fully charged) to adequately handle the peaks that occur early in the time-series residential/commercial load data, while the constraint in Eq. (20) requires the terminal energy in-store to be greater than or equal to the initial energy in-store for the sake of balanced analysis. In addition, for reasons of computational efficiency, linear upper bound constraints were imposed on the decision variables (size of the components) in line with the potential physical limitations, as expressed in Eq. (21) [61,62].

$$E_B(0) = N_B \times C_{B,r}, \tag{19}$$

$$E_B(T) \ge E_B(0), \tag{20}$$

$$0 \le N_c \le N_c^{max}, \quad \forall c \tag{21}$$

2.3.3. Overview of the dispatch strategy

Fig. 2 provides a flowchart of the overall dispatch strategy developed to effectively coordinate the scheduling of the distributed energy resources integrated into the MGs based on a set of pre-defined rules. It is noteworthy that the most efficient strategy for charging or not charging EV batteries using the stationary BESS depends on the connectedness to the main grid, specific circumstances of the charging system and the renewable energy sources available. It is important to carefully consider all of these factors when designing and implementing a charging system for EVs. The preliminary results from this study revealed that slightly overbuilding renewables would be more cost-effective than using the energy stored in the stationary BESS to charge EV batteries during periods of low solar and wind generation. The reader is referred to Appendix B for the mathematical formulations of the devised dispatch strategy.

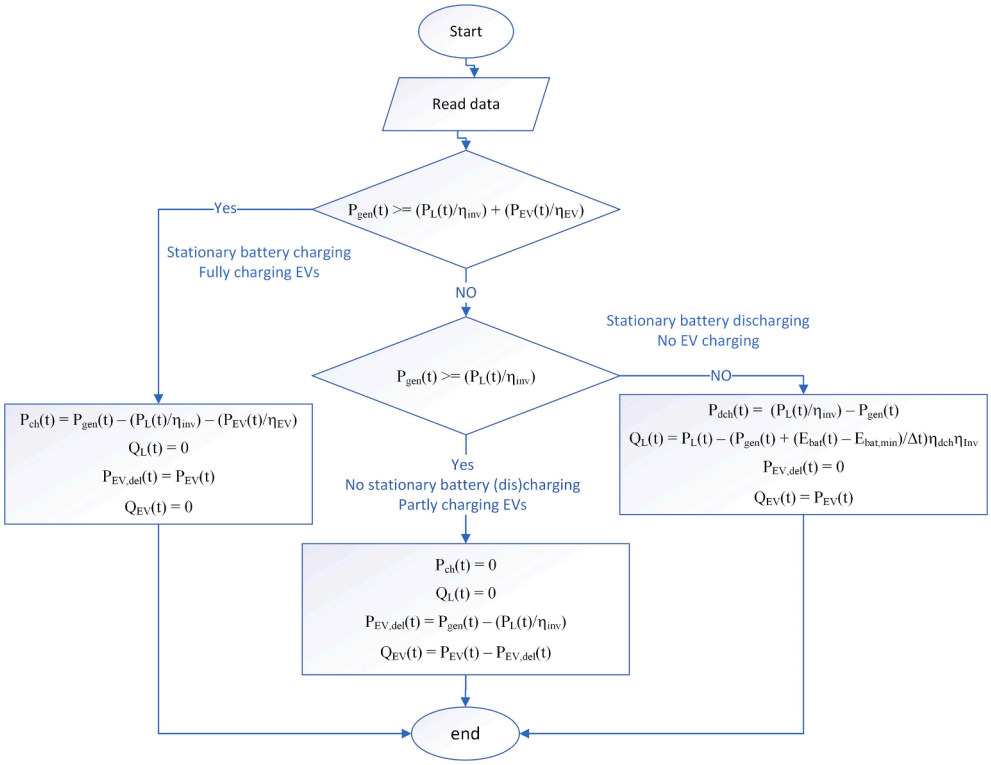

Fig. 2. Flowchart of the proposed EV-addressable rule-based MG energy dispatch strategy.

2.4. Availability of generation components

To provide an additional layer of reliability, the expected forced outage rates of solar PV panels and WTs were modelled. To this end, it was assumed that they are associated with fixed availability probabilities of 96% [63]. The probability of being in each availability state can be determined using a binomial density function [63]. For instance, the probability of being in a state associated with the failure of n solar panels, n_{PV}^{fail}, out of the total N solar panels installed, N_{PV}, and the failure of n WTs, n_{WT}^{fail}, out of the total N WTs installed, N_{WT}, can be calculated as [63]:

$$f_{gen}\left(n_{PV}^{fail}, n_{WT}^{fail}\right) = \left[\left(\frac{N_{PV}}{n_{PV}^{fail}}\right) \times A_{PV}^{N_{PV}-n_{PV}^{fail}} \times (1-A_{PV})^{n_{PV}^{fail}}\right] \times \left[\left(\frac{N_{WT}}{n_{WT}^{fail}}\right) \times A_{WT}^{N_{WT}-n_{WT}^{fail}} \times (1-A_{WT})^{n_{WT}^{fail}}\right], \quad (22)$$

where A_{PV} and A_{WT} respectively denote the availability of each solar PV panel and each WT.

Given that a stochastic approach is employed to characterise the uncertainties in all the time series input data (refer to Section 2.6), adding another uncertainty quantification dimension would have made the simulations overly computationally complex – and possibly intractable. Therefore, it was decided to simplify the modelling of the availability of non-dispatchable generation components. To this end, following the procedure described in [63], first the equivalent renewable power generation space considering the associated forced outage rates was derived as:

$$P_{gen}^{eq} = E\left[P_{gen}\right] = \sum_{s \in S} P_{gen}(s) \times f_{gen}(s), \quad (23)$$

where $s \in S$ represents the discretised search space.

Then, substituting Eq. (22) into Eq. (23), the equivalent renewable power generation space for the problem under consideration can be re-written as [63]:

$$P_{gen}^{eq} = \sum_{n_{PV}^{fail}=0}^{N_{PV}} \sum_{n_{WT}^{fail}=0}^{N_{WT}} \left[P_{gen}\left(n_{PV}^{fail}, n_{WT}^{fail}\right) \times f_{gen}\left(n_{PV}^{fail}, n_{WT}^{fail}\right)\right]. \quad (24)$$

Finally, following the steps undertaken in [63], Eq. (24) can be simplified as:

$$P_{gen}^{eq} = N_{PV} \times P_{PV} \times A_{PV} + N_{WT} \times P_{WT} \times A_{WT}. \quad (25)$$

It should also be noted that given that the battery and inverter are normally installed in indoor enclosures [64], their failures can safely be assumed negligible.

2.5. Demand response: EV-charging loads

To improve the load factor and thereby minimise the risks of sub-optimal designs due to unnecessary excess curtailments, a new DR scheme is considered for the coordination of EV-charging loads. To this end, the EV loads are treated as deferrable loads, the effective dispatching of which is expected to help minimise the system-wide mismatches between variable generation and total load demand – thereby reducing the infrastructure capacity needed to serve the peak load alone.

It is assumed that each EV owner specifies the arrival time and departure time and the amount of energy required to reach the desired battery state-of-charge, in accordance with Fig. 3. The DR mechanism then seeks to find the optimum time for charging each EV within the specified driving pattern and constraints of EV use, as displayed in Fig. 3. To this end, inspired by the general idea of modelling shiftable loads originally proposed by Amrollahi and Bathaee [65], first, the on/off status of EV-charging at each time-step within the user-specified period of time is represented as [65]:

$$\sum_{t=AT_k}^{DP_k} Status_k(t) = Availability_k, \quad \forall k \quad (26)$$

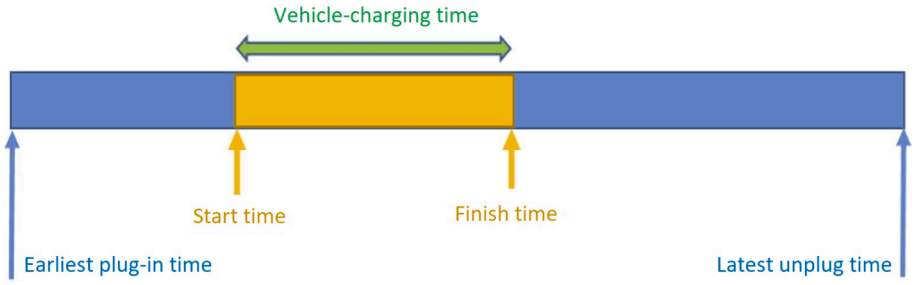

Fig. 3. Illustration of the availability constraints of EVs (adapted from [65]).

where AT_k and DP_k respectively denote the arrival time and departure time of the k-th EV, *Status* is a binary variable which controls whether the EV is charging or not (1 represents charging, 0 not charging), while *Availability* is the timespan over which the EV needs to be charged.

Also, to prevent the occurrence of charging and not charging decisions at a single time-step, the following constraint is imposed, which defines the relationship between the charging and idle modes of EV while plugged in [65]:

$$Ch_k(t) + Nch_k(t) \leq 1, \quad \forall t, \forall k \tag{27}$$

where Ch_k corresponds to the *Status* variable taking a value of 1 (charging the k-th EV); Nch_k a value of 0 (not charging the EV).

Each EV-charging load can then be shifted forward or backward within the pre-defined availability time period and the associated constraints, as illustrated in Fig. 4. The forward and backward shifting of the EV loads can also be conducted in a consecutive or non-consecutive manner [66].

Under these assumptions, the daily power consumption scheduling vector of each vehicle $k \in K$ within the MG service territory is given by [67]:

$$P_k = \left[p_k^1, \cdots, p_k^{24}\right], \quad \forall k \tag{28}$$

Based on the customer-specified total daily EV-charging load, P_k^{total}, and the plug-in availability period, the following vehicle-specific equality constraint needs to be met [67]:

$$P_k^{total} = \sum_{t=AT_k}^{DT_k} p_k^t . Status_k(t). \tag{29}$$

Within these constraints, the overall EV-charging shifting matrix can be developed as [67]:

$$S_k^{total} = \begin{bmatrix} p_k^1 & p_k^{24} & p_k^{23} & \cdots & p_k^2 \\ \vdots & \vdots & \vdots & \ddots & \vdots \\ p_k^{24} & p_k^{23} & p_k^{22} & \cdots & p_k^1 \end{bmatrix}. \tag{30}$$

Furthermore, each EV-charging power should lie within a specified range, in accordance with the minimum and maximum allowable charging capacity specifications of the corresponding EV's battery, as [67]:

$$p_k^{min} \leq p_k(t) \leq p_k^{max}, \quad \forall t, \forall k \tag{31}$$

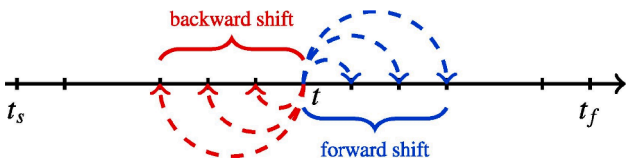

Fig. 4. Illustration of the forward and backward shifting of EV-charging loads within the constraints of mobility use (adapted from [66]).

2.6. Uncertainty quantification

To systematically characterise the multi-dimensional uncertainties inherent in the problem, the formulated deterministic problem is transformed into a stochastic version. More specifically, the uncertainties in forecasts of solar irradiance, ambient temperature, wind speed (where appropriate), as well as residential and commercial loads are quantified using a novel uncertainty characterisation approach based on probability density function (PDF) discretisation. To this end, first, the best-fitting distributions for the aforementioned uncertainty factors are built. Table 2 presents the PDF used for each random variable of interest.

Subsequently, the continuous PDFs of the time-step-specific uncertain parameters are approximated by a number of equal-width discrete intervals, and are represented by the means of those intervals and the associated probabilities of occurrence. The associated discretisation process of the PDFs is illustrated in Fig. 5.

The following equations represent the probabilities and the associated uncertain parameter values of the discrete approximations [72]:

$$p_i = \int_{R_i} \{x\} dx \qquad for \quad i = 1, \quad 2, \quad \ldots, \quad 7, \tag{32}$$

$$x_i = \int_{R_i} x \frac{\{x\}}{p_i} dx \qquad for \quad i = 1, \quad 2, \quad \ldots, \quad 7, \tag{33}$$

where R_i denotes the i-th region on the corresponding PDF's value axis.

Then, based on all possible combinations of the time-step-specific intervals, a number of multi-dimensional scenario vectors are generated. For the uncertainty factors under consideration, the scenario vector is $SV(t) = [G_T(t), T_a(t), v(t), P_L(t)]$.

Table 2
Determination of the best-fitting PDFs of the stochastic parameters.

Parameter	PDF	Mathematical model	Source
Solar irradiance	Beta	$f(x) = \frac{\Gamma(\alpha+\beta)}{\Gamma(\alpha)\Gamma(\beta)} x^{\alpha-1}(1-x)^{\beta-1}$, where $\alpha, \beta > 0$ are the shape parameters and $\Gamma(z)$ is the gamma function.	[68]
Ambient temperature	Normal	$f(x) = \frac{1}{\sqrt{2\pi}\sigma} e^{\frac{1}{2}\left(\frac{x-\mu}{\sigma}\right)^2}$, where μ denotes the mean and σ is the standard deviation.	[68,69]
Load demand	Normal	$f(x) = \frac{1}{\sqrt{2\pi}\sigma} e^{\frac{1}{2}\left(\frac{x-\mu}{\sigma}\right)^2}$, where μ denotes the mean and σ is the standard deviation.	[69,70]
Wind speed	Weibull	$f(x) = \frac{k}{c}\left(\frac{x}{c}\right)^{k-1} e^{\left(\frac{x}{c}\right)^k}$, where $k > 0$ is the shape parameter and c > 0 is the scale parameter.	[69,70]

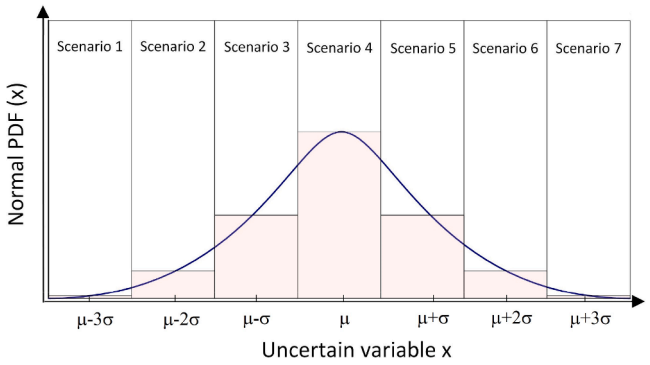

Fig. 5. Discretising a representative Gaussian PDF based on equal-width regions (adapted from [71]).

To alleviate the computational burden, the mixed-integer linear programming (MILP)-based scenario reduction technique [73] is used, which can be formulated as follows:

$$\min N_s = \sum_{x_1=1}^{Nd}\sum_{x_2=1}^{Nd}\sum_{x_3=1}^{Nd}\sum_{x_4=1}^{Nd}\omega_{x_1,x_2,x_3,x_4}, \tag{34}$$

subject to:

$$\sum_{x_2=1}^{Nd}\sum_{x_3=1}^{Nd}\sum_{x_4=1}^{Nd}p_s(x_1,\ x_2,\ x_3,\ x_4) = p_{1,x_1},\ x_1 = 1,\ 2,\cdots,\ Nd \tag{35}$$

$$\sum_{x_1=1}^{Nd}\sum_{x_3=1}^{Nd}\sum_{x_4=1}^{Nd}p_s(x_1,\ x_2,\ x_3,\ x_4) = p_{2,x_2},\ x_2 = 1,\ 2,\cdots,\ Nd \tag{36}$$

$$\sum_{x_1=1}^{Nd}\sum_{x_2=1}^{Nd}\sum_{x_4=1}^{Nd}p_s(x_1,\ x_2,\ x_3,\ x_4) = p_{3,x_3},\ x_3 = 1,\ 2,\cdots,\ Nd \tag{37}$$

$$\sum_{x_1=1}^{Nd}\sum_{x_2=1}^{Nd}\sum_{x_3=1}^{Nd}p_s(x_1,\ x_2,\ x_3,\ x_4) = p_{4,x_4},\ x_4 = 1,\ 2,\cdots,\ Nd \tag{38}$$

$$\sum_{x_1=1}^{Nd}\sum_{x_2=1}^{Nd}\sum_{x_3=1}^{Nd}\sum_{x_4=1}^{Nd}p_s(x_1,\ x_2,\ x_3,\ x_4) = 1,\ \forall x_1,\ x_2,\ x_3,\ x_4 \tag{39}$$

$$p_s(x_1,\ x_2,\ x_3,\ x_4) \le \omega_{x_1,x_2,x_3,x_4},\quad \forall x_1,\ x_2,\ x_3,\ x_4 \tag{40}$$

$$0 \le p_s(x_1,\ x_2,\ x_3,\ x_4) \le 1,\quad \forall x_1,\ x_2,\ x_3,\ x_4 \tag{41}$$

where N_s is the number of reduced scenarios, Nd is the number of discrete intervals, ω_{x_1,x_2,x_3,x_4} is a binary variable that represents the presence of each scenario, $p_s(x_1,\ x_2,\ x_3,\ x_4)$ is the new probability associated with the reduced scenario vector, while p_{n,x_n} denotes the probability that the n-th uncertainty factor takes on the value of x_n.

Finally, the deterministic model is simulated for the set of reduced scenario vectors, with the expected value of the minimised objective function and the resulting values of the decision variables representing the uncertainty-aware solutions in the most likely scenario.

2.7. Overview of the proposed method

Fig. 6 shows a flowchart of the proposed method. First, all input data, including scalars and historical time series are loaded. The green blocks represent the uncertainty characterisation components of the model. To characterise the uncertainties, first, the hour-specific PDFs are generated for each variable time-series input. Subsequently, multi-dimensional scenario vectors are generated and reduced. The model then proceeds to run the deterministic model for each reduced scenario for the optimum equipment mix using the selected metaheuristic.

The metaheuristic-based processes are represented by blue blocks in Fig. 6. Specifically, for each search agent of the metaheuristic algorithm, the proposed DR scheduling framework that uses the flexibility potential of EV-charging loads is run on a day-ahead basis (the yellow block) before applying the devised rule-based dispatch strategy on an hourly basis (the light coral block). Finally, for each scenario, the globally optimum values of the total discounted system cost and size of the components are recorded, the expected values of which represent the most likely results under multi-dimensional uncertainty. It is also noteworthy that the selected metaheuristics are integrated into the proposed solution approach on an individual basis. Moreover, the process of updating the positions of the search agents of the metaheuristics in an iterative manner is continued until reaching the maximum number of iterations as the stopping criterion.

Furthermore, Fig. 7 illustrates how different model components build upon each other. Specifically, at the innermost layer of the model lies the proposed rule-based dispatch strategy, which is aware of the fact that serving EV loads using the energy stored in the stationary battery is not energy efficient. The day-ahead demand-side management layer, built on the hourly dispatch strategy layer, then seeks to shift the EV-charging loads to maximise the load factor subject to the EV owners' comfort constraints. The constraints on the operation and planning of the MG, to which the optimal solution must adhere are then defined. Finally, the objective function representing the total net present cost is formulated and minimised in a probabilistic manner to effectively account for the uncertainties involved. The figure also shows the key input data that need to be processed before use, as well as the key outputs of the model.

3. Case study: Input data

This section presents the input data supplied to the proposed model for three case communities residing on Aotea–Great Barrier Island, in Aotearoa–New Zealand, namely: Medlands, Tryphena, and Mulberry Grove. First, the overall geographical and climatic conditions of the case study sites are briefly described. The section then proceeds to more specifically detail the meteorological and energy consumption data forecasts before presenting a summary of the scalars used within the model.

Fig. 8 shows the geographical locations of the three communities considered for off-grid MG installations. In terms of geographical location, Mulberry Grove and Tryphena are about 6.3 km and 8.1 km from Medlands, respectively. Accordingly, MG 1 is populated for the case of Medlands, whereas MG 2 is populated for the cases of Tryphena (MG 2a) and Mulberry Grove (MG 2b). For more detailed background information on the case study refer to the Supplementary Material accompanying the paper (Additional File 2: Case study background information and time-series data).

3.1. Techno-economic specifications

Table 3 presents a summary of the assumed values for the technical and cost parameters of the components of the MGs and the associated sources. Note that all costs are in 2021 New Zealand Dollars and were derived from the local renewable energy asset market in the years 2020 and 2021[1]. Furthermore, the project lifetime and the expected interest rate were respectively assumed to be 25 years and 3.7%. The interest rate was estimated by taking the average over the last 10 years, from 2012 to 2021 [74].

Also, Table 4 presents the values of the parameters used within the model, including those related to the mathematical models of the components integrated, as well as the operational- and planning-level constraints.

3.2. Specifications of metaheuristics

Table 5 presents the adjusted values for the parameters of the metaheuristics in the candidate pool, in accordance with the associated

[1] Mean NZD to USD exchange rate in 2021 [95]: 1 NZD = 1.41 USD.

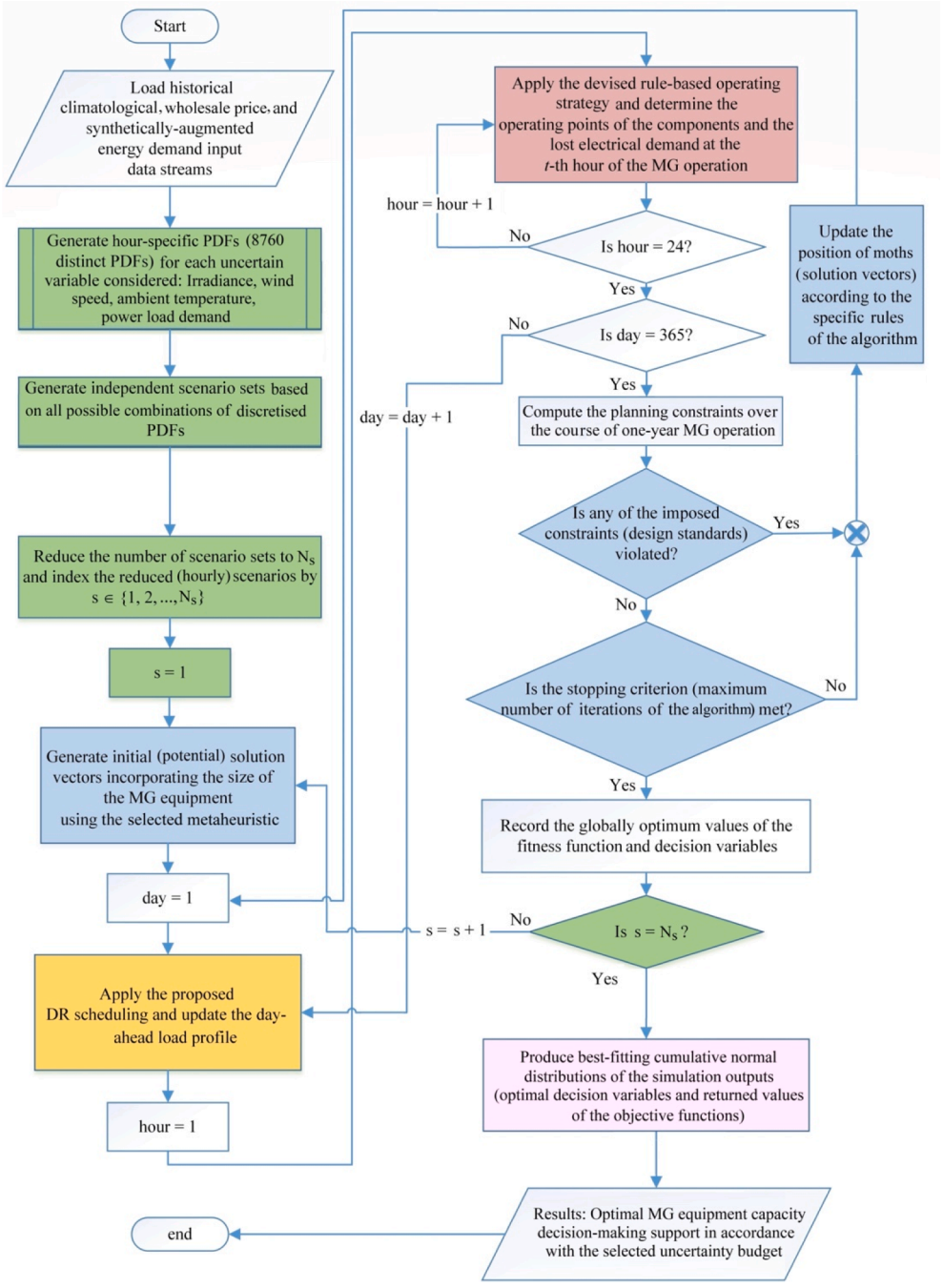

Fig. 6. Flowchart of the proposed stochastic off-grid MG sizing method considering EV-charging demand-side management.

developer-suggested values for multi-dimensional problems. A detailed description of the parameters used in each algorithm is provided in the Supplementary Material (Additional File 3: Overview of the selected metaheuristics). Also, the number of search agents and the maximum number of iterations were respectively fixed at 100 and 200 for all metaheuristics under consideration to enable a fair comparison.

4. Simulation results and discussion

This section discusses the numerical simulation results derived from coding the proposed method parametrised for the three MG test-cases modelled, which were populated for the corresponding three sites of interest. The model was simulated using the MATLAB R2022a software [89] on a standard desktop computer. The reader is referred to the Supplementary Material accompanying the paper (Additional File 4: Model validation) for additional energy flow, cash flow, and capital budgeting analyses, which reinforce the validity of the proposed method.

4.1. Performance comparison of the selected algorithms

A new method was used to rank the performance of the metaheuristics of interest in MG equipment capacity planning applications. The proposed ranking technique incorporates the following five descriptive statistics: the standard deviation, mean, and median of the total net present costs (TNPCs) yielded throughout the literature-standard 30 independent simulation runs, as well as the associated best- and worst-case results out of the 30 trials of optimising a solution to

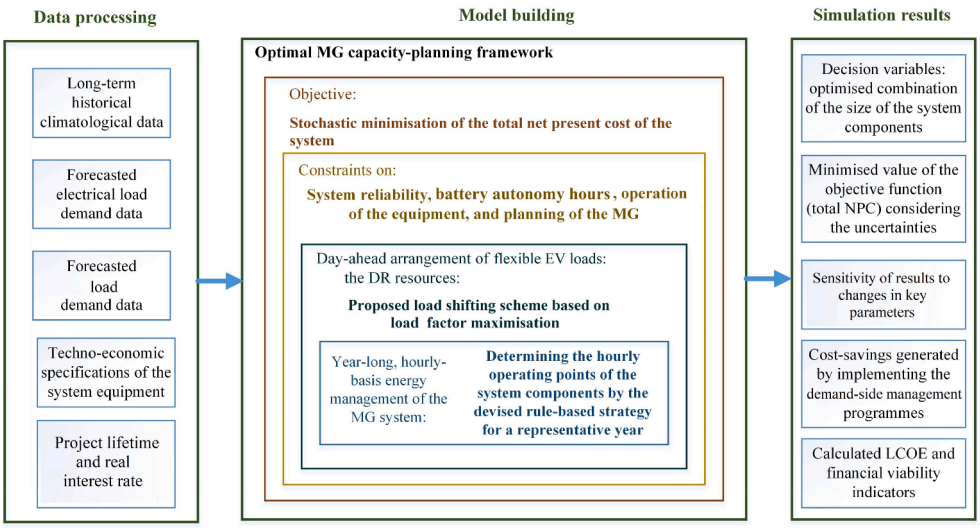

Fig. 7. Illustration of the layer-by-layer structure of the proposed method.

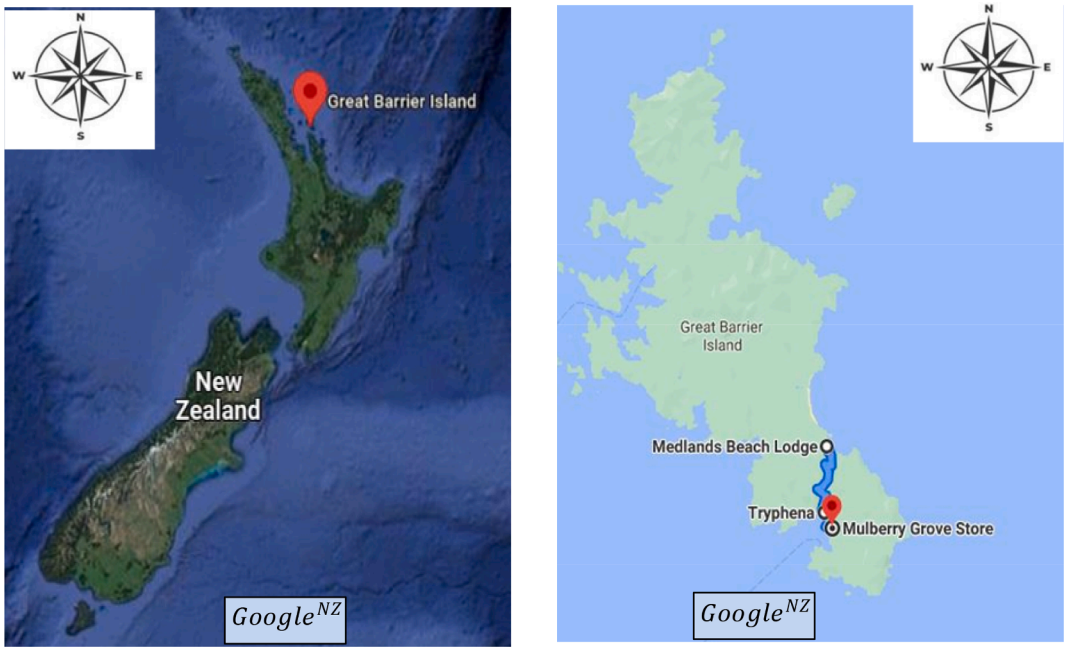

Fig. 8. Locations of the conceptualised MGs for installation on Aotea–Great Barrier Island (image courtesy of Google Earth™ mapping service).

Table 3
Techno-economic specifications of the MG components.

Component	Nameplate rating (generic)	Capital cost	Replacement cost	O&M cost	Expected life	Efficiency	Source
WT	50 kW	$59k/unit	$45k/unit	$800/unit/year	25 years	N/A[a]	[75]
Solar PV	330 W	$350/unit	$220/unit	$5/unit/year	25 years	17.5%	[76]
BESS	14 kWh	$14k/unit	$9k/unit	$30/unit/year	15 years	95%[b]	[77]
AC/DC converter[d]	50 kW	$4.5k/unit	$4k/unit	$28/unit/year	15 years	98%	[78]
DC/DC converter[d]	360 W	$50/unit	$50/unit	$1/unit/year	15 years	97%	[79,80]
Inverter	21 kW	$8k/unit	$8k/unit	$320/unit/year	20 years	96%[c]	[80]
EV charger	7.6 kW	$4k/unit	$4k/unit	$160/unit/year	20 years	99%	[81]

[a] Not applicable as the WT's efficiency is controlled by the approximated power curve.
[b] Individual charge and discharge efficiencies.
[c] Expected value, as the inverter efficiency is modelled dynamically (in a power output-dependent manner).
[d] In the optimisation model, the costs and efficiencies of the AC/DC and DC/DC converters were respectively integrated into the costs and effectiveness of the WTs and the solar PV panels/battery bank in the interests of reducing the dimensionality of the overall problem at hand.

Table 4
Summary of the parameter settings of the overall model.

Scalar	Value	Scalar	Value	Scalar	Value
PV panels		*Inverter*		$LPSP_L^{min}$	100%
η_{pc}	97%	η_{10}	94.5%	$LPSP_{EV}^{min}$	100%
μ	− 0.48%/°C	η_{100}	92.5%	AD_{bat}^{min}	24 h
NOCT	43 °C	*Battery*		A_{PV}	96%
$T_{a.NOCT}$	20 °C	$C_{B.r}$	14 kWh	A_{WT}	96%
$G_{T.NOCT}$	800 W/m^2	P_{ch}^{min}	0 kW	N_{PV}^{max}	10,000
$T_{c.ref}$	25 °C	P_{dch}^{max}	5 kW	N_{WT}^{max}	2,000
Wind turbines		σ	1.5%/month	N_B^{max}	100
v_r	9.5 m/s	P_{dch}^{min}	0 kW	N_{inv}^{max}	1,000
v_{cut-in}	3.5 m/s	P_{dch}^{max}	5 kW	*Overall model*	
$v_{cut-out}$	20 m/s	DOD^{max}	95%	Δt	1 h
P_r	50 kW	*Constraints*		*Nd*	7

Table 5
Parameter settings of the examined metaheuristics.

Metaheuristic	Parameter settings	Source
PSO	Acceleration constants = 2, inertia weight = 0.7	[82]
MFOA	Constant defining the shape of the logarithmic spiral = 1	[83]
WHO	Crossover percentage = 0.1	[84]
AHA	Probability of performing either the guided foraging or the territorial foraging = 50%	[85]
AGTO	Parameter defining the exploitation power = 0.8	[86]
MPA	Ratio between the encounter rates for the Lévy and Brownian predators = 0.1	[87]
EO	Generation probability = 0.5	[88]

the three MG sizing problems.

The standard deviation measures the amount of variation or dispersion of the population of TNPC outputs, while the mean of the set of TNPC observations represents the arithmetic average of the values – and indicates the central tendency of the values. Also, the median is the value separating the higher half of the population of TNPC outputs from the lower half. The mean of the results, as well as the best- and worst-case solutions, indicate the accuracy of the algorithms under comparison, whereas the median and standard deviation values indicate the precision of the algorithms over 30 independent trials.

Table 6 presents the total discounted system costs obtained from the application of the algorithms, the comparative efficiency of which is under investigation, to the optimal equipment capacity planning problem of the three MG instances over 30 simulation runs. The rank order of the algorithms is determined by taking the average of the descriptive statistics for each MG sizing case first (Avg. 1) – which determines the case-specific scores of metaheuristics when applied to the optimal MG sizing problems of interest – and then taking the average of the resulting scores over the three cases (Avg. 2). The following points should be noted for a better interpretation of the comparative results presented in Table 6:

- Low standard deviation values indicate that data are clustered around the mean (i.e., the data values are concentrated close to the mean), whereas high standard deviation indicates that data are more spread out (i.e., the data values show more variation from the mean).
- A standard deviation equal to zero indicates that there is no spread in data.
- When the mean value is greater than the median value, the distribution curve is skewed to the right (positively skewed). On the other hand, when the median value is greater than the mean value, the distribution curve is skewed to the left (negatively skewed).
- The best- and worst-case values respectively indicate the minimum and maximum TNPCs obtained over 30 independent simulation runs.

The comparative results presented in Table 6 are revealing in the following ways:

- The MFOA and the EO have the best and worst performances, respectively. More specifically, the summary-statistics-based metaheuristic comparison framework confirms that the MFOA

Table 6
Summary-statistics-based efficiency comparison of the selected metaheuristics applied to the three MG planning cases in terms of the total net present cost ($).

Alg.	Sys.	St. Dev.	Best	Worst	Mean	Median	Avg. 1	Score	Avg. 2	Rank
PSO	MG 1	1,523	438,177	444,152	439,070	438,611	440,003	6		
	MG 2a	126	426,553	427,241	426,576	426,553	426,731	4	5	5
	MG 2b	974	272,791	278,123	272,968	272,791	274,168	5		
MFOA	MG 1	296	425,539	426,589	425,651	425,539	425,830	1		
	MG 2a	218	413,689	413,720	413,223	413,218	413,462	1	1	1
	MG 2b	0	256,754	257,000	256,754	256,754	256,816	1		
WHO	MG 1	37,689	438,171	515,553	468,126	438,171	465,005	5		
	MG 2a	1	426,553	426,554	426,553	426,553	426,553	7	6	6
	MG 2b	1	272,791	272,792	272,791	272,791	272,791	6		
AHA	MG 1	106	435,838	436,287	435,972	435,944	436,010	3		
	MG 2a	737	431,073	434,475	431,265	431,075	431,972	6	4	4
	MG 2b	1	266,999	267,004	267,001	267,000	267,001	3		
AGTO	MG 1	256	435,791	436,546	435,945	435,804	436,021	2		
	MG 2a	1	431,073	431,074	431,073	431,073	431,073	5	3	2
	MG 2b	1	266,999	267,000	266,999	266,999	266,999	2		
MPA	MG 1	1	438,171	438,173	438,171	438,171	438,171	4		
	MG 2a	1	426,553	426,554	426,553	426,553	426,553	2	3.33	3
	MG 2b	1	272,791	272,793	272,791	272,791	272,791	4		
EO	MG 1	2,400	438,186	445,214	439,341	438,219	440,240	7		
	MG 2a	1	426,553	426,554	426,553	426,553	426,553	3	5.66	7
	MG 2b	0	272,791	272,793	272,791	272,791	272,791	7		

Table 7
Optimal designing results for the three cases optimised by the selected algorithms in their best performance.

Algorithm	Sys.	PVs (no.)	WTs (no.)	BESS (no.)	Inverter (kW)	TNPC ($)
PSO	MG 1	127	3	11	59	438,177
	MG 2a	792	N/A[a]	7	53	426,553
	MG 2b	541	N/A[a]	4	40	272,791
MFOA	MG 1	102	3	10	59	425,539
	MG 2a	784	N/A[a]	7	53	413,689
	MG 2b	523	N/A[a]	4	40	256,754
WHO	MG 1	127	3	11	59	438,171
	MG 2a	792	N/A[a]	7	53	426,553
	MG 2b	541	N/A[a]	4	40	272,791
AHA	MG 1	209	2	12	59	435,838
	MG 2a	796	N/A[a]	8	53	431,073
	MG 2b	536	N/A[a]	4	40	266,999
AGTO	MG 1	208	2	12	59	435,791
	MG 2a	796	N/A[a]	8	53	431,073
	MG 2b	536	N/A[a]	4	40	266,999
MPA	MG 1	127	3	11	59	438,171
	MG 2a	792	N/A[a]	7	53	426,553
	MG 2b	541	N/A[a]	4	40	272,791
EO	MG 1	127	3	11	59	438,186
	MG 2a	792	N/A[a]	7	53	426,553
	MG 2b	541	N/A[a]	4	40	272,791

[a] N/A = No wind power generation is considered in MGs 2a and 2b.

outperforms the other six algorithms investigated, namely the PSO, the WHO, the AHA, the AGTO, the MPA, and the EO. The utilisation of the MFOA for the optimal sizing of the cases of interest reduces the expected TNPC in the best run by $12,647 (~3%), $12,864 (~3%), and $16,037 (~6%) for MG 1, MG 2a, and MG 2b, respectively, compared to the EO, which is the least well-performing metaheuristic.

- The standard deviation of the TNPC outputs of the MFOA and the EO when applied to the third MG are both equal to 0. This indicates the robustness of the MFOA in yielding the globally optimal solution, whilst substantiating the comparative inefficiency of the EO in MG planning applications.
- Based on the Avg. 2 metric, the following rank order can be established for the metaheuristics under comparison: the MFOA > the AGTO > the MPA > the AHA > the PSO > the WHO > the EO.

Furthermore, Table 7 presents the optimal capacities of the candidate technologies for the three cases, which represent the best-case performance of the metaheuristics considered. It can be observed from the table that, compared to the AHA and the AGTO, the MFOA allocates more WTs in the case of MG 1 to reduce the size of the battery storage capacity. Also, although the number of WTs selected by the MFOA for MG 1 is equal to those optimised by the PSO, the WHO, the MPA, and the EO, it returns comparatively lower capacities for the solar PV generation system and the BESS. This can be explained by the MFOA's unique feature of dynamically rebalancing exploration – the early stages of the optimisation process that represents the long-range movement of search agents – for improved exploitation – the local search around promising regions of the search space identified in the exploration phase. Such a rebalancing procedure is found to be particularly useful for optimising a solution in the general multi-dimensional, nonlinear, non-convex shape of the decision space of MG sizing problems.

It is also worth recalling that the size of the inverter does not constitute part of the solution set in the optimisation procedure, as it is calculated exogenously (outside the model) based on the peak load demand. It should also be noted that the optimal size of each component is rounded up to the nearest integer given the continuous nature of the selected metaheuristics. The associated TNPCs were, accordingly, rounded up to the nearest integer.

Fig. 9 depicts the convergence curves of the selected metaheuristics in their best runs when applied to MG 1. It can be observed from the figure that the MFOA, the AGTO, and the MPA have almost the same convergence behaviour, whereas the AHA, the PSO, and the WHO take more iterations to converge. The figure also reveals that the weaker performance of the EO can be explained by its premature trapping in poor local optima. These observations collectively confirm the comparable simulation speed of the MFOA to the fastest metaheuristics in the candidate pool that are associated with comparable efficiencies, namely the AGTO and the MPA.

Given the demonstrated outperformance of the MFOA to the other metaheuristics investigated in the candidate pool, as well as the

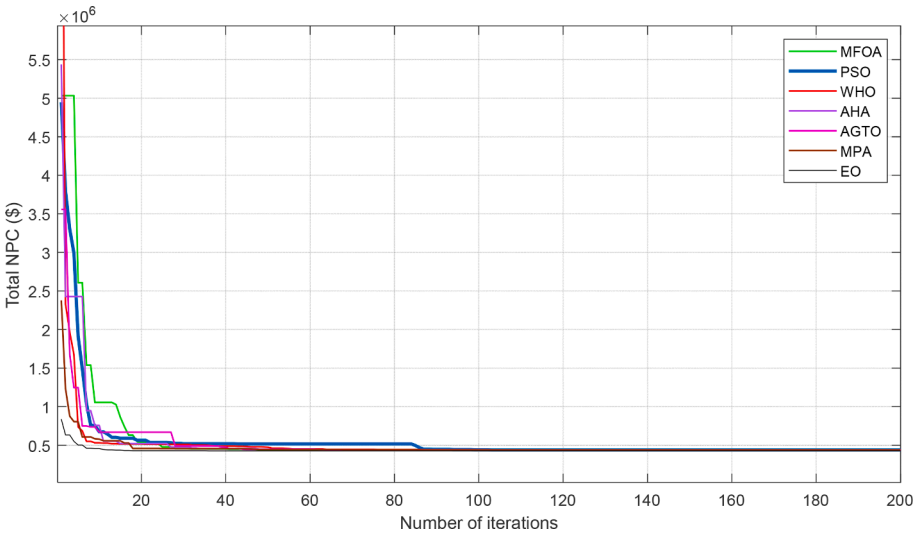

Fig. 9. Best-case convergence curves of the selected metaheuristics when applied to MG 1.

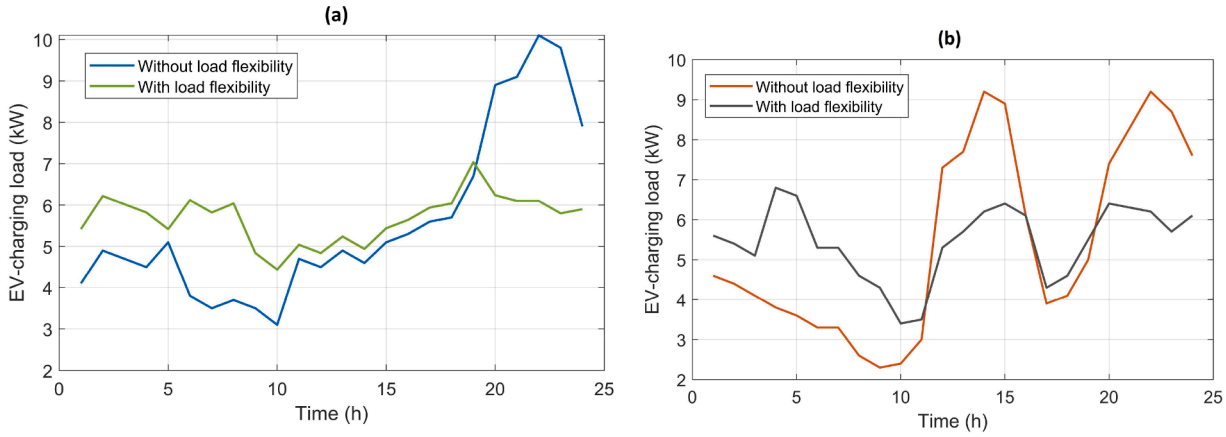

Fig. 10. Impact of load shifting on the EV-charging load profiles for: (a) MG 1, and (b) MGs 2a and 2b.

negligibly low standard value of the returned value of the objective function over 30 independent trials, all the following analyses are undertaken based on the best-performance run of the MFOA.

4.2. Impact of EV-charging flexibility

Fig. 10 shows the impact of running the proposed scheme for the flexible serving of EV load demand on the shape of the aggregate EV load on MGs 1, 2a, and 2b for typical daily charging patterns. As the figure shows, the proposed scheme leads to flattening the aggregate MG-wide EV-charging load profiles, which in turn, reduces the peak-to-average ratio of the overall load profile and improves the load factor. Specifically, applying the proposed scheme has shaved ~29%, ~24%, and ~24% off the EV load profiles of MGs 1, 2a, and 2b, respectively. Consequently, this has led to a peak shaving of ~18%, ~15%, and ~13%, respectively, on the corresponding overall load demand profiles made up of both appliance and EV loads. Accordingly, the overall peak-to-average ratios of the overall load profiles of MGs 1, 2a, and 2b are reduced by ~31%, ~26%, and ~23%, respectively.

To further clarify the impact of the proposed EV-oriented DR model on the load power demand data used in the optimal capacity planning algorithm, Fig. 11 presents the monthly average 24-hour electricity consumption profile for the cases with and without DR for MG 1. The figure shows that implementing the proposed DR model results in reducing the maximum peak power demand by a significant 38%. This, in turn, leads to an increase in the load factor – the ratio of the average power demand to the maximum power demand – from 0.30 in the baseline case to 0.41 in the case with DR.

Table 8 presents the comparative optimal sizing results for the three cases under consideration with and without shifting the EV-charging loads to off-peak hours subject to the constraints imposed by the mobility patterns of EV owners. As the table shows, leveraging the flexibility potential of EV loads is able to substantially reduce the total discounted system cost given the significant contribution of the EV loads to the overall demand. Specifically, it has reduced the TNPC of the system by ~25% (equating to ~$107k), ~25% (~$103k), and ~27% (~$70k) in MGs 1, 2a, and 2b, respectively. The table is also revealing in two ways in terms of the impact of EV demand-side management on the size of the components, namely:

1. While the lowering of the EV peak demand significantly reduces the need for over-building of renewable generation which would only be used during times of highest demand, it does not materially change the size of stationary storage needed. This can be mainly explained by the fact that onsite battery storage is not used to charge the EVs' batteries, and that no DR programme is considered for appliance loads.
2. Expectedly, given that EV-charging loads are addressed using level-1 chargers, the EV load shifting has a significant impact on the size of the inverter. It should be noted that given the zero unmet load constraint imposed, the size of the inverter directly reflects the magnitude of the peak load shaved. A comparison of the residential/commercial and EV-charging load profiles (refer to Additional File 2 in Supplementary Material accompanying the paper) indicates a large evening peak in both profiles across the three cases. This is the main underlying reason for the reduced size of the inverter following the shifting of the charging of EVs to off-peak hours.

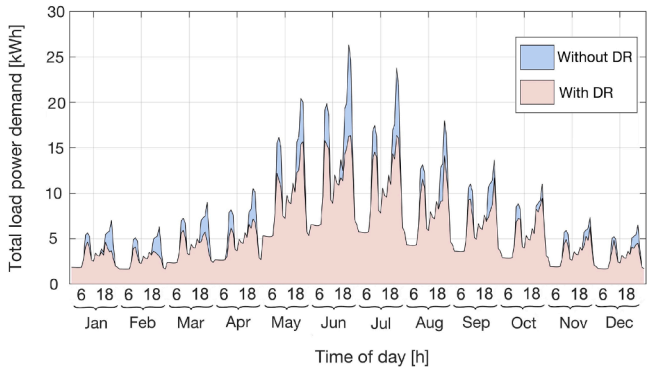

Fig. 11. Illustration of the impact of the proposed EV-oriented DR strategy on the overall monthly mean daily (24-hour) load profile of MG 1.

Furthermore, a comparison of the solution sets in the two scenarios indicates a considerable reduction of the percentage of excess renewable generation curtailed where EV-load shifting schemes are present, and hence the overbuilt generation capacity that would be rarely used. This, consequently, has improved the economics of the overall systems. It is worth recalling that only the excess renewable generation is directed towards serving the EV loads given the absence of a utility grid and the inefficiency of battery-to-battery charging processes.

4.3. Economics of energy resilience

To measure the relative importance of energy resilience in 100%-renewable MGs tailored to remote and isolated areas, comprehensive sensitivity analyses were performed. To this end, the changes in the total discounted system cost of MG 1 (in the case without flexible EV-charging loads) were quantified against the changes in the minimum allowed battery autonomy days. More specifically, the deterministic optimisation was run using increasing levels of the battery autonomy hours from 1 day to 10 days in intervals of 1 day.

Fig. 12 depicts the sensitivity of the system TNPC to changes in the

Table 8
Comparison of the optimal sizing results with and without EV demand-side management.

Scenario	MG	PVs (no.)	WTs (no.)	BESS (no.)	Inverter (kW)	Total cost ($)	Percentage of curtailed generation
Without EV-charging flexibility	MG 1	102	3	10	59	425,539	10%
	MG 2a	784	N/A	7	53	413,689	14%
	MG 2b	523	N/A	4	40	256,754	11%
With EV-charging flexibility	MG 1	85	2	9	48	319,478	4%
	MG 2a	589	N/A	6	41	310,450	6%
	MG 2b	390	N/A	3	36	187,010	5%

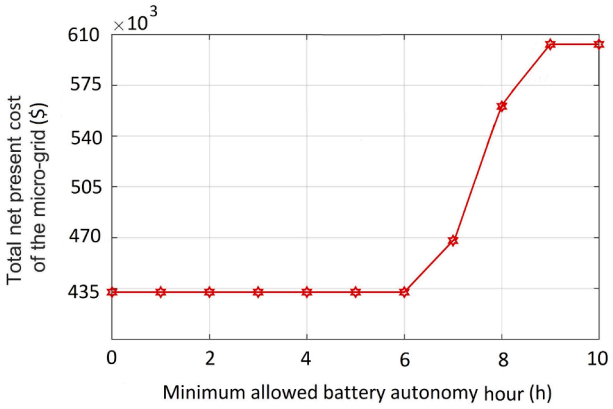

Fig. 12. Sensitivity of the TNPC of MG1 (without EV-charging flexibility) to changes in minimum allowed battery autonomy hours.

Table 9
Comparative costings and configurations of MG 1 under various minimum allowed resilience constraints.

Sensitivity case	PVs (no.)	WTs (no.)	BESS (no.)	Inverter (kW)	Total cost ($)	Percentage of curtailed generation
0	102	3	10	59	425,539	10%
1	102	3	10	59	425,539	7%
2	102	3	10	59	425,539	5%
3	102	3	10	59	425,539	3%
4	102	3	10	59	425,539	3%
5	102	3	10	59	425,539	2%
6	102	3	10	59	425,539	12%
7	127	3	11	59	459,214	15%
8	138	4	11	59	558,851	16%
9	154	4	12	59	595,410	21%
10	154	4	12	59	595,410	21%

specified battery autonomy hour constraint for the three cases under consideration. It can be observed from the figure that in all the cases, the TNPC is particularly sensitive to increases in the battery autonomy hour above 6 days. That is, the TNPC increases monotonically with increasing autonomy required, but not necessarily strictly monotonically or linearly. For example, a significantly sharper increase in the total discounted system cost is expected for the designs with battery autonomy days of 8 days compared to those with battery autonomy days of 7 days. This can be largely attributed to the need for larger capacities of renewable power generation required and the associated interactions with the excess generation curtailments.

For greater insights into the relationships between the excess generation curtailment and the economics of energy resilience, Table 9 presents the detailed MG 1 sizing results for the sensitivity cases considered with respect to the minimum allowed battery autonomy hour. As the table indicates, increasing the battery autonomy from 1 day to 5 days is associated with reductions in the percentage of curtailed generation as the extra battery capacity is primarily charged using the otherwise-curtailed excess generation. However, the case with 6 battery autonomy days represents a turning point in terms of how the excess generation is dealt with.

More specifically, from a battery autonomy of 6 days onwards the excess generation curtailed starts to increase. This is mainly due to the need for adding more renewable power capacities under such more conservative constraints solely for resilience reasons, which practically play no part in serving the loads during normal operating conditions. In other words, highly conservative solutions in terms of renewables outage survivability not only necessitate oversized storage capacities, but also imply relatively largely underutilised renewable capacities – as gradual charging of the stationary battery storage using excess generation would not be sufficient in those cases. The general insight emerging from the above observations is that there exists a critical point, beyond which increasing the resilience more drastically deteriorates the economics of a 100%-renewable off-grid power supply. Such a point can be viewed as a reasonable trade-off (best compromise) between cost and resilience.

4.4. *Effects of uncertainty*

To evaluate the effects of uncertainty on the optimal solutions, the deterministic and stochastic results in the presence of EV-charging load flexibility are compared in Table 10. In the stochastic model variant, the underlying parametric uncertainties are quantified using the proposed multi-dimensional uncertainty characterisation approach. As the table shows, failure to account for the variability inherent in the relevant time-series data would have led to an underestimation of the total discounted system cost by ~24% (equating to ~$102k), ~21% (~$81k), and ~19% (~$43k) respectively in MGs 1, 2a, and 2b. The reason for a slightly higher impact of the uncertainty characterisation on the estimated total discounted cost of MG 1 is the presence of WTs in the candidate pool which necessitates the characterisation of the uncertainty in wind speed forecasts. In other words, MG 1 is associated with four sources of parametric uncertainty compared to the three addressed for MGs 2a and 2b – solar irradiance, temperature, and load demand. Another potential contributing factor to the more pronounced impact of uncertainty modelling on the results of MG 1 is its comparatively larger scale, which potentially results in widened mismatches between load and generation.

Also, in terms of impact on the optimal component mix, the characterisation of uncertainties has increased the optimal capacity of the solar PV system by as much as ~8% (equating to 2.3 kW), ~12% (23.8 kW), and ~15% (19.5 kW) in MGs 1, 2a, and 2b, respectively. Furthermore, for the WTs integrated into MG 1, the uncertainty characterisation has increased the overall capacity required by a significant 50% (equating to 50 kW). It is noteworthy that the effective distribution of uncertainty reduction-related added renewable capacities (which has given more weight to the increase in the size of the WT generation system), as well as leveraging the associated power generation complementarities, are the main two reasons behind the relatively smaller increase in the optimal capacity of the solar PV generation system in MG 1.

Moreover, the optimal capacity of the BESS is found to be less sensitive to the variability of renewables and load demand. This can be mainly attributed to the fact that the EV-charging load, which cannot be

Table 10
Comparison of the deterministic and stochastic results considering flexible EV-charging loads.

Model output	Deterministic results			Stochastic results		
	MG 1	MG 2a	MG 2b	MG 1	MG 2a	MG 2b
PVs (no.)	85	589	390	92	661	449
WTs (no.)	2	N/A	N/A	3	N/A	N/A
BESS (no.)	9	6	3	11	8	4
Inverter (kW)	48	41	36	60	52	48
Total cost ($)	319,478	310,450	187,010	421,374	391,291	230,372
Percentage of curtailed generation	4%	6%	5%	5%	8%	6%

met using stationary battery discharges, is a substantial contributor to the overall load demand. The presence of a minimum allowed self-sufficiency ratio also contributes to the lower sensitivity of the battery size to the system-wide uncertainties, albeit to a lesser degree compared to the aforementioned large share of EV-charging power consumption. The effect of uncertainties on the total capacity of the inverter system is, additionally, directly correlated with the changes in the peak net power demand due to the characterisation of uncertainties.

5. Conclusions and future work

This paper has presented a novel probabilistic, resilience-oriented, EV-charging DR-integrated MG sizing method tailored to off-grid MGs, particularly solar PV/WT/battery and solar PV/battery systems. Using insights from an Aotearoa–New Zealand case study, the model has generalised the long-term strategic MG capacity planning optimisation problem in four important areas, namely:

- The state-of-the-art metaheuristics have a significant potential to improve the economics of MGs, which can be leveraged to pave the way towards a renewables-based economy. More specifically, based on multi-case-study analyses, it has been found that the MFOA could outperform the leading metaheuristic in MG sizing applications, the PSO algorithm, by approximately 6% – with significant potential cost savings in mid- to large-scale off-grid MG developments. Also, the descriptive statistics-based rank order of the examined metaheuristics has been found to be as: the MFOA > the AGTO > the MPA > the AHA > the PSO > the WHO > the EO.
- The EV-charging load is the largest contributor to the overall demand in an electrified transport scenario. Therefore, it is not optimal to charge EVs when arriving home from work as it exacerbates the evening peak load and, in turn, increases the peak capacity needed, which would then be substantially underutilised. Accordingly, an efficient load-shifting programme is needed to shift the EV loads to off-peak hours subject to the constraints imposed by the mobility patterns of EV owners, thereby flattening the overall load profile. For the cases considered, the proposed EV-load-addressable DR programme has improved the economics of the designed MGs by a significant ~26%, on average.
- Ignoring the forecast uncertainties can result in significant degrees of deviation from reality. That is, failure to account for the system-wide parametric uncertainties can necessitate more expensive reinforcing or even reengineering of the system. It is, therefore, essential to holistically address the multivariate nature of the uncertainty sources. The multi-variant quantitative evidence from the studied cases has demonstrated the effectiveness of the proposed general framework for the probabilistic characterisation of the uncertainties involved in producing financially robust MG designs.
- Sensitivity analyses performed based on the proposed model have also demonstrated that the value that the target communities place on energy resilience has a significant influence on the total discounted cost of grid-isolated MGs. More specifically, considering the battery autonomy days as the resilience metric, increasing the required resilience from 1 day to 10 days increases the total cost of the system by at least ~40%. This poses a significant barrier to the deployment of 100%-renewable energy systems in remote and isolated areas. Therefore, effective trade-offs between system cost and energy resilience are of significant importance during the planning phase.

In conclusion, the paper has shown the importance of resilience considerations and coordinated EV charging management during the long-term strategic planning of off-grid MGs tailored to communities that currently suffer from security of supply issues associated with standalone diesel generator systems. It has also substantiated the importance of a systematic multi-case-study-oriented, uncertainty-aware method for robust conclusions around the performance of metaheuristics in the MG sizing problem.

Future work is also planned for a more integrative variant of the proposed model, where (i) the flexibility potential of residential/commercial appliances is effectively utilised, (ii) the coalitional behaviour of off-grid utility enterprises and residential/commercial end-consumers is modelled using insights from cooperative game theory to effectively capture the interactions between different parties involved, (iii) the uncertainties in techno-economic specifications, such as the inflation rate and replacement costs of infrastructures are factored in, and (iv) the degradation of EV batteries is factored in to better account for the performance and cost implications of EVs on the economic viability of MGs. Future work could also explore the integration of various energy vectors on a broader level – beyond MGs focused exclusively on electricity – and compare the performance of the selected *meta*-heuristics when applied to more complex MG configurations. This could involve investigating the potential for heat, cooling, hydrogen, and other forms of energy carriers, into a comprehensive system that maximises energy efficiency and minimises environmental impact. Such an integrated approach would provide a more holistic understanding of the challenges and opportunities for sustainable energy and could help aid associated investment decisions towards a more sustainable energy future.

CRediT authorship contribution statement

Soheil Mohseni: Conceptualization, Methodology, Data curation, Formal analysis, Investigation, Resources, Software, Validation, Visualization, Writing – original draft. **Roomana Khalid:** Data curation, Investigation, Resources, Software, Visualization. **Alan C. Brent:** Supervision, Project administration, Formal analysis, Investigation, Resources, Validation, Writing – review & editing.

Declaration of Competing Interest

The authors declare that they have no known competing financial interests or personal relationships that could have appeared to influence the work reported in this paper.

Data availability

Data will be made available on request.

Appendix A. Mathematical formulation of the components

This appendix presents the mathematical formulations of the components of the conceptualised MGs.

A1. Solar PV

The power output from each solar PV panel at each time-step of the simulation, t, can be obtained from the following equation [54,55]:

$$P_{PV}(t) = \eta A_s G_T(t), \tag{A.1}$$

where A_s denotes the surface area of each panel (m^2), G_T represents the total solar irradiance (W/m^2), while η represents the time-variant overall PV system efficiency which can be calculated using Eq. (A.2) [54,55].

$$\eta(t) = \eta_r \eta_{pc} \left[1 - \mu\left(T_c(t) - T_{c,ref}\right)\right], \tag{A.2}$$

where η_r denotes the reference module efficiency, η_{pc} is the efficiency of the internal power converter, μ denotes the temperature coefficient of power of PV cells (%/°C), $T_{c,ref}$ is the reference cell temperature (°C), and $T_c(t)$ represents the temperature of PV cells at time-step t, which is given by [54,55]:

$$T_c(t) = T_a(t) + [(NOCT - T_{a,NOCT})/G_{T,NOCT}]G_T(t), \tag{A.3}$$

where $NOCT$ is the nominal operating cell temperature, $T_{a,NOCT}$ and $G_{T,NOCT}$ respectively denote the ambient temperature and total solar irradiance at the normal operation conditions, with $T_a(t)$ denoting the ambient temperature (°C).

A2. Wind turbines

The power output from each WT can be expressed as a function of wind speed as [90,91]:

$$P_{WT}(t) = \begin{cases} \left((Av(t))^3 + B\right)P_r, & v_{cut-in} \le v(t) < v_r \\ P_r, & v_r \le v(t) \le v_{cut-out} \\ 0, & otherwise \end{cases} \tag{A.4}$$

where P_r is the rated power output of the turbine, $v(t)$ denotes the wind speed, v_{cut-in} is the cut-in wind speed, $v_{cut-out}$ is the cut-out wind speed, while A and B are constants which can be defined as [90,91]:

$$A = \frac{1}{v_r^3 - v_{cut-in}^3}, \tag{A.5}$$

$$B = \frac{v_{cut-in}}{v_r^3 - v_{cut-in}^3}. \tag{A.6}$$

Fig. A1 illustrates the equations used for modelling the power output of WTs with respect to wind speed [65].

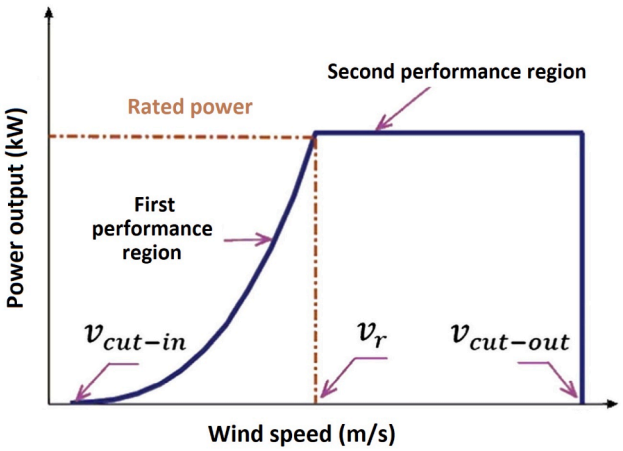

Fig. A1. Illustration of the power curve of a typical representative WT (adapted from [65]).

A3. Battery

The battery bank is the only dispatchable component in both system configurations, and thereby serves as the primary source for balancing the supply of demand within the systems under consideration. To this end, the energy content of the battery bank is used to couple each time-step to other time increments. That is, the power outputs from wind and solar PV generators are used to determine when the battery should charge or discharge. Accordingly, the following equation gives the battery bank energy content at each time-step [92]:

$$E_{bat}(t) = \begin{cases} E_{bat}(t-1)(1-\sigma) + (\eta_{ch} P_{ch}(t))\Delta t, & charging\ mode \\ E_{bat}(t-1)(1-\sigma) - (P_{dch}(t)/\eta_{dch})\Delta t, & discharging\ mode \end{cases} \quad (A.7)$$

where $E_{bat}(t-1)$ is the battery energy content at the previous time-step, σ denotes the hourly self-discharge rate, η_{ch} is the charging efficiency, η_{dch} is the discharging efficiency, P_{ch} is the charging power, P_{dch} is the discharging power, with Δt representing the duration of each time-step which is used to convert the unit of power to energy.

In accordance with the standard practice in long-term strategic MG planning studies, it is assumed that the degradation of the stationary battery storage is linear.

Accordingly, the remaining capacity of the battery bank as a function of the cycles it has undergone, can be calculated as [93]:

$$C_b(cycles) = C_{ini} - \frac{C_{ini} - C_{last}}{Cycles_{max}} \times cycles, \quad (A.8)$$

where C_{ini} is the capacity of the battery at the first cycle, C_{last} is the capacity of the battery at the last cycle, while $Cycles_{max}$ is the battery bank's expected maximum number of cycles.

The process for the calculation of the remaining capacity of the battery bank as a function of the cycles it has undergone is also illustrated in Fig. A2.

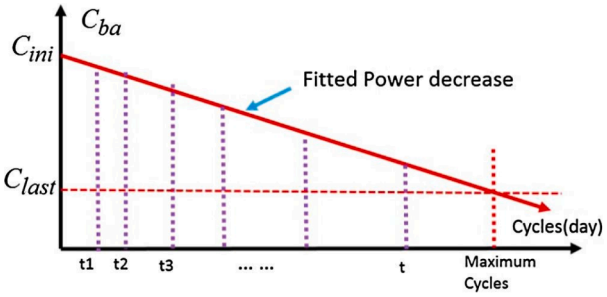

Fig. A2. Illustration of the remaining capacity of the battery bank with respect to the number of cycles (adapted from [93]).

A4. Inverter

To better reflect reality, a dynamic model was used for the inverter, whereby the efficiency of the inverter can be obtained as follows [94]:

$$\eta_{inv} = \frac{P}{P + P_0 + kP^2}, \quad (A.9)$$

where P, P_0, and k are defined as:

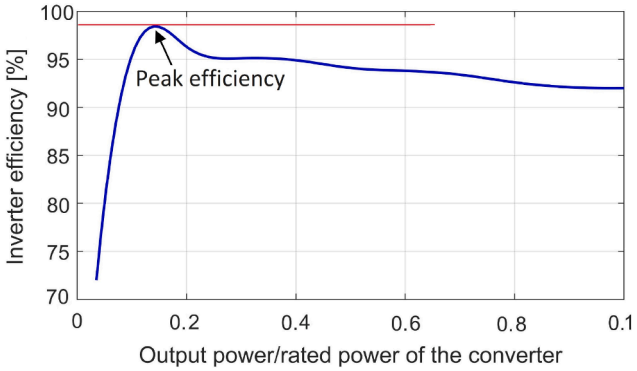

Fig. A3. Illustration of the output power-dependent efficiency of the inverter.

$$P = \frac{P_{out}}{P_{in}}, \tag{A.10}$$

$$P_0 = 1 - 99(\frac{10}{\eta_{10}} - \frac{1}{\eta_{100}} - 9)^2, \tag{A.11}$$

$$k = \frac{1}{\eta_{100}} - P_0, \tag{A.12}$$

where η_{10} and η_{100} denote the manufacturer-provided inverter efficiencies at 10% and 100% of its nameplate rating.

Fig. A3 illustrates the equations used for modelling the output power of the inverter with respect to its dynamic efficiency for varying output power to rated power ratios.

Appendix B. Dispatch strategy

This appendix formulates the proposed dispatch strategy for the operation of the MGs of interest. To effectively handle the peak demand coincident with the charging of EVs, a specific rule-based dispatch strategy was developed. For energy efficiency considerations, the dispatch strategy does not supply the energy demand of EV loads from the battery bank's energy in store. Accordingly, depending on the status of aggregate variable renewable generation, P_{gen}, aggregate non-EV load demand, P_L, and aggregate EV-charging load demand, P_{EV}, three dispatch scenarios may occur, which are defined and formulated mathematically in the following sections.

B1. Renewable power generation equals total demand

This case assumes the total power output from variable renewables to be equal to the sum of aggregate non-EV and EV load demands, which can be mathematically modelled as:

$$P_{PV}(t) + P_{WT}(t) = P_L(t)/\eta_{inv} + P_{EV}(t)/\eta_{EV}, \tag{B.1}$$

$$E_b(t + \Delta t) = E_b(t), \tag{B.2}$$

$$P_{EV,del}(t) = P_{EV}(t), \tag{B.3}$$

where $P_{EV,del}$ is the actual power delivered to EVs at time-step t and η_{EV} denotes the efficiency of EV chargers.

B2. Excess renewable power generation

In this scenario, it is primarily assumed that the total variable renewable power generation exceeds the aggregate load on the MG. Accordingly, any surplus variable renewable power generation is dispatched to the BESS for later use. The operational strategy of the system can be mathematically modelled as:

$$P_{ch}(t) = P_{PV}(t) + P_{WT}(t) - (P_L(t)/\eta_{inv}) - (P_{EV}(t)/\eta_{EV}), \tag{B.4}$$

$$E_b(t + \Delta t) = E_b(t-1) + P_{ch}(t) \times \eta_{ch} \times \Delta t, \tag{B.5}$$

$$P_{EV,del}(t) = P_{EV}(t). \tag{B.6}$$

A second if-statement subsequently checks whether the onsite variable renewable power generation is not able to supply the entire demand on the MG but there exists excess generation with respect to the non-EV loads alone (residential and commercial loads). In such circumstances, the associated excess generation is used to serve the EV-charging loads as far as possible, which can be modelled as:

$$P_{EV,del}(t) = P_{PV}(t) + P_{WT}(t) - (P_L(t)/\eta_{inv}), \tag{B.7}$$

$$Q_{EV}(t) = P_{EV}(t) - P_{EV,del}(t), \tag{B.8}$$

where Q_{EV} is the lost EV-charging load, which can be obtained by subtracting the actual power delivered to the EVs' batteries from the expected total EV load demand, as expressed in Eq. (B.8).

Also, it is assumed that where it is not possible to store the excess power in the battery bank due to the energy and/or power capacity limits, the amount of overflown energy is spilled or dumped.

B3. Renewable power deficit

This scenario assumes that the total non-EV load demand is larger than the aggregate variable renewable power generation. Accordingly, the energy stored in the BESS is withdrawn to supply the non-EV loads to the greatest extent possible. However, the total EV load demand is remained unmet, which results in the loss of total EV loads, Q_{EV}, in addition to some part or whole of the non-EV loads, Q_{load}. This scenario can be mathematically modelled as:

$$P_{dch}(t) = (P_L(t)/\eta_{inv}) - P_{PV}(t) - P_{WT}(t), \tag{B.9}$$

$$E_b(t+\Delta t) = E_b(t-1) - (P_{dch}(t)/\eta_{dch}) \times \Delta t, \tag{B.10}$$

$$P_{EV,del}(t) = 0, \tag{B.11}$$

$$Q_{EV}(t) = P_{EV}(t). \tag{B.12}$$

As can be seen from Eqs. (B.11) and (B.12), the EV-charging load remains entirely unserved during the periods where residential and commercial loads exceed the total renewable power generation.

Where non-EV load shedding is necessary to maintain the power balance of the system due to the depletion of the battery storage and/or inadequacy of its power capacity, the associated lost residential and commercial loads can be obtained from the following equation:

$$Q_L(t) = P_L(t) - \left(P_{PV}(t) + P_{WT}(t) + \left(\frac{E_b(t) - E_b^{min}}{\Delta t}\right) \times \eta_{dch}\right) \times \eta_{inv}. \tag{B.13}$$

More specifically, in this scenario, the onsite storage is used to its maximum capacity to meet the residential and commercial loads. Yet, despite doing so, there exists unserved demand, apart from unsupplied EV-charging loads, which should be accounted for as lost load in the associated reliability calculations.

Appendix C. Supplementary material

Supplementary data to this article can be found online at https://doi.org/10.1016/j.apenergy.2023.121007.

References

[1] Warneryd M, Håkansson M, Karltorp K. Unpacking the complexity of community microgrids: A review of institutions' roles for development of microgrids. Renew Sustain Energy Rev 2020;121:109690.

[2] Hussain A, Bui VH, Kim HM. Microgrids as a resilience resource and strategies used by microgrids for enhancing resilience. Appl Energy 2019;240:56–72.

[3] Fioriti D, Poli D, Duenas-Martinez P, Micangeli A. Multiple design options for sizing off-grid microgrids: A novel single-objective approach to support multi-criteria decision making. Sustain Energy Grids Netw 2022:100644.

[4] Castillo-Calzadilla T, Macarulla AM, Kamara-Esteban O, Borges CE. A case study comparison between photovoltaic and fossil generation based on direct current hybrid microgrids to power a service building. J Clean Prod 2020;244:118870.

[5] Mashayekh S, Stadler M, Cardoso G, Heleno M. A mixed integer linear programming approach for optimal DER portfolio, sizing, and placement in multi-energy microgrids. Appl Energy 2017;187:154–68.

[6] Atia R, Yamada N. Sizing and Analysis of Renewable Energy and Battery Systems in Residential Microgrids. IEEE Trans Smart Grid 2016;7(3):1204–13.

[7] Li B, Roche R, Miraoui A. Microgrid sizing with combined evolutionary algorithm and MILP unit commitment. Appl Energy 2017;188:547–62.

[8] Castillo-Calzadilla T, Macarulla AM, Kamara-Esteban O, Borges CE. Analysis and assessment of an off-grid services building through the usage of a DC photovoltaic microgrid. Sustain Cities Soc 2018;38:405–19.

[9] Castillo-Calzadilla T, Cuesta MA, Olivares-Rodriguez C, Macarulla AM, Legarda J, Borges CE. Is it feasible a massive deployment of low voltage direct current microgrids renewable-based? A technical and social sight. Renew Sustain Energy Rev 2022;161:112198.

[10] Emad D, El-Hameed MA, Yousef MT, El-Fergany AA. Computational Methods for Optimal Planning of Hybrid Renewable Microgrids: A Comprehensive Review and Challenges. Arch Comput Methods Eng 2020;27(4):1297–319.

[11] Yang X-S. Nature-inspired metaheuristic algorithms. Luniver Press; 2008.

[12] Yang X-S. Engineering optimization: an introduction with metaheuristic applications. John Wiley & Sons; 2010.

[13] Nagapurkar P, Smith JD. Techno-economic optimization and social costs assessment of microgrid-conventional grid integration using genetic algorithm and Artificial Neural Networks: A case study for two US cities. J Clean Prod 2019;229:552–69.

[14] Diab AAZ, El-Rifaie AM, Zaky MM, Tolba MA. Optimal Sizing of Stand-Alone Microgrids Based on Recent Metaheuristic Algorithms. Mathematics 2022;10(1):140.

[15] Maleki A, Pourfayaz F. Optimal sizing of autonomous hybrid photovoltaic/wind/battery power system with LPSP technology by using evolutionary algorithms. Sol Energy 2015;115:471–83.

[16] Peng W, Maleki A, Rosen MA, Azarikhah P. Optimization of a hybrid system for solar-wind-based water desalination by reverse osmosis: Comparison of approaches. Desalination 2018;442:16–31.

[17] Maleki A, Askarzadeh A. Comparative study of artificial intelligence techniques for sizing of a hydrogen-based stand-alone photovoltaic/wind hybrid system. Int J Hydrogen Energy 2014;39(19):9973–84.

[18] Fathi M, Khezri R, Yazdani A, Mahmoudi A. Comparative study of metaheuristic algorithms for optimal sizing of standalone microgrids in a remote area community. Neural Comput Appl 2022;34(7):5181–99.

[19] Bukar AL, Tan CW, Lau KY. Optimal sizing of an autonomous photovoltaic/wind/battery/diesel generator microgrid using grasshopper optimization algorithm. Sol Energy 2019;188:685–96.

[20] Sukumar S, Marsadek M, Ramasamy A, Mokhlis H. Grey Wolf Optimizer Based Battery Energy Storage System Sizing for Economic Operation of Microgrid, 2018 IEEE International Conference on Environment and Electrical Engineering and 2018 IEEE Industrial and Commercial Power Systems Europe (EEEIC/I&CPS Europe); 2018, pp. 1-5.

[21] Abo-Elyousr FK, Guerrero JM, Ramadan HS. Prospective hydrogen-based microgrid systems for optimal leverage via metaheuristic approaches. Appl Energy 2021;300:117384.

[22] Hemmati R, Mehrjerdi H, Nosratabadi SM. Resilience-oriented adaptable microgrid formation in integrated electricity-gas system with deployment of multiple energy hubs. Sustain Cities Soc 2021;71:102946.

[23] Bajwa AA, Mokhlis H, Mekhilef S, Mubin M. Enhancing power system resilience leveraging microgrids: A review. J Renew Sustain Energy 2019;11(3):035503.

[24] Wang Y, Rousis AO, Strbac G. On microgrids and resilience: A comprehensive review on modeling and operational strategies. Renew Sustain Energy Rev 2020;134:110313.

[25] Kamara-Esteban O, et al. Bridging the Gap between Real and Simulated Environments: A Hybrid Agent-Based Smart Home Simulator Architecture for Complex Systems. In: 2016 Intl IEEE Conferences on Ubiquitous Intelligence & Computing, Advanced and Trusted Computing, Scalable Computing and Communications, Cloud and Big Data Computing, Internet of People, and Smart World Congress (UIC/ATC/ScalCom/CBDCom/IoP/SmartWorld); 2016. p. 220–7.

[26] Castillo-Calzadilla T, Macarulla AM, Borges CE. Design of Sizing Algorithms for a Direct Current Off-Grid Photovoltaic Installation. IEEE Lat Am Trans 2018;16(8):2168–76.

[27] Marqusee J, Becker W, Ericson S. Resilience and economics of microgrids with PV, battery storage, and networked diesel generators. Adv Appl Energy 2021;3:100049.

[28] Masrur H, Sharifi A, Islam MR, Hossain MA, Senjyu T. Optimal and economic operation of microgrids to leverage resilience benefits during grid outages. Int J Electr Power Energy Syst 2021;132:107137.

[29] Anderson KH, DiOrio NA, Cutler DS, Butt RS. Increasing resiliency through renewable energy microgrids. Int J Energy Sect Manag 2017;2. NREL/JA-7A40-69034.

[30] Wang Y, Rousis AO, Strbac G. Resilience-driven optimal sizing and pre-positioning of mobile energy storage systems in decentralized networked microgrids. Appl Energy 2022;305:117921.

[31] Martins VF, Borges CLTT. Active Distribution Network Integrated Planning Incorporating Distributed Generation and Load Response Uncertainties. IEEE Trans Power Systems 2011;26(4):2164–72.

[32] Ehrenmann A, Smeers Y. Stochastic equilibrium models for generation capacity expansionStochastic optimization methods in finance and energy. Springer; 2011. p. 273–310.

[33] Kahrobaee S, Asgarpoor S, Qiao W. Optimum sizing of distributed generation and storage capacity in smart households. IEEE Trans Smart Grid 2013;4(4):1791–801.

[34] Cardoso G, et al. Optimal investment and scheduling of distributed energy resources with uncertainty in electric vehicle driving schedules. Energy 2013;64:17–30.

[35] Salyani P, Abapour M, Zare K, Babri T. Optimal Stochastic Planning of DERs in a Game Theory Framework Considering Demand Response and Pollution Issues. In: Nojavan S, Zare K, editors. Demand Response Application in Smart Grids: Concepts and Planning Issues -, Volume 1. Cham: Springer International Publishing; 2020. p. 193–214.

[36] Basu M. Optimal generation scheduling of hydrothermal system with demand side management considering uncertainty and outage of renewable energy sources. Renew Energy 2020;146:530–42.

[37] Farrokhifar M, Aghdam FH, Alahyari A, Monavari A, Safari A. Optimal energy management and sizing of renewable energy and battery systems in residential sectors via a stochastic MILP model. Electr Power Syst Res 2020;187:106483.

[38] Sugimura M, et al. Optimal sizing and operation for microgrid with renewable energy considering two types demand response. J Renew Sustain Energy 2020;12(6):65901.
[39] Amir V, Azimian M. Dynamic Multi-Carrier Microgrid Deployment Under Uncertainty. Appl Energy 2020;260:114293.
[40] Mansouri SA, Ahmarinejad A, Javadi MS, Catalão JPS. Two-stage stochastic framework for energy hubs planning considering demand response programs. Energy 2020;206:118124.
[41] Mansouri SA, Ahmarinejad A, Ansarian M, Javadi MS, Catalão JPS. Stochastic planning and operation of energy hubs considering demand response programs using Benders decomposition approach. Int J Electr Power Energy Syst 2020;120:106030.
[42] Yang X, Chen Z, Huang X, Li R, Xu S, Yang C. Robust capacity optimization methods for integrated energy systems considering demand response and thermal comfort. Energy 2021;221:119727.
[43] Zeng B, Liu Y, Xu F, Liu Y, Sun X, Ye X. Optimal demand response resource exploitation for efficient accommodation of renewable energy sources in multi-energy systems considering correlated uncertainties. J Clean Prod 2021;288:125666.
[44] Wagner R, Antoniou I, Pedersen SM, Courtney MS, Jørgensen HE. The influence of the wind speed profile on wind turbine performance measurements. Wind Energy: An Int J Progr Appl Wind Power Convers Technol 2009;12(4):348–62.
[45] Martinot E. Grid integration of renewable energy: flexibility, innovation, and experience. Annu Rev Environ Resour 2016;41.
[46] Rabiee A, Sadeghi M, Aghaeic J, Heidari A. Optimal operation of microgrids through simultaneous scheduling of electrical vehicles and responsive loads considering wind and PV units uncertainties. Renew Sustain Energy Rev 2016;57:721–39.
[47] Li Y, Li K. Incorporating Demand Response of Electric Vehicles in Scheduling of Isolated Microgrids With Renewables Using a Bi-Level Programming Approach. IEEE Access 2019;7:116256–66.
[48] Sedighizadeh M, Shaghaghi-shahr G, Esmaili M, Aghamohammadi MR. Optimal distribution feeder reconfiguration and generation scheduling for microgrid day-ahead operation in the presence of electric vehicles considering uncertainties. J Energy Storage 2019;21:58–71.
[49] Liu C, et al. Stochastic scheduling of a renewable-based microgrid in the presence of electric vehicles using modified harmony search algorithm with control policies. Sustain Cities Soc 2020;59:102183.
[50] Castillo-Calzadilla T, Alonso-Vicario A, Borges CE, Martin C. E-Mobility in Positive Energy Districts. Buildings 2022;12(3):pp.
[51] Haupt L, Schöpf M, Wederhake L, Weibelzahl M. The influence of electric vehicle charging strategies on the sizing of electrical energy storage systems in charging hub microgrids. Appl Energy 2020;273:115231.
[52] Mortaz E, Vinel A, Dvorkin Y. An optimization model for siting and sizing of vehicle-to-grid facilities in a microgrid. Appl Energy 2019;242:1649–60.
[53] Harsh P, Das D. Optimal coordination strategy of demand response and electric vehicle aggregators for the energy management of reconfigured grid-connected microgrid. Renew Sustain Energy Rev 2022;160:112251.
[54] Huld T, Gottschalg R, Beyer HG, Topič M. Mapping the performance of PV modules, effects of module type and data averaging. Sol Energy 2010;84(2):324–38.
[55] Borhanazad H, Mekhilef S, Gounder Ganapathy V, Modiri-Delshad M, Mirtaheri A. Optimization of micro-grid system using MOPSO. Renew Energy 2014;71:295–306.
[56] Hakimi SM, Hasankhani A, Shafie-khah M, Catalão JPS. Optimal sizing and siting of smart microgrid components under high renewables penetration considering demand response. IET Renew Power Gener 2019;13(10):1809–22.
[57] Bhamidi L, Sivasubramani S. Optimal Planning and Operational Strategy of a Residential Microgrid With Demand Side Management. IEEE Syst J 2019;14(2):1–9.
[58] Shin J, Lee JH, Realff MJ. Operational planning and optimal sizing of microgrid considering multi-scale wind uncertainty. Appl Energy 2017;195:616–33.
[59] Radosavljević J, Jevtić M, Klimenta D. Energy and operation management of a microgrid using particle swarm optimization. Eng Optim 2016;48(5):811–30.
[60] Maleki A, Askarzadeh A. Artificial bee swarm optimization for optimum sizing of a stand-alone PV/WT/FC hybrid system considering LPSP concept. Sol Energy 2014;107:227–35.
[61] Alharbi H, Bhattacharya K. Stochastic optimal planning of battery energy storage systems for isolated microgrids. IEEE Trans Sustain Energy 2018;9(1):211–27.
[62] Zhu T, Lot R, Wills RGA, Yan X. Sizing a battery-supercapacitor energy storage system with battery degradation consideration for high-performance electric vehicles. Energy 2020;208:118336.
[63] Baghaee HR, Mirsalim M, Gharehpetian GB. Multi-objective optimal power management and sizing of a reliable wind/PV microgrid with hydrogen energy storage using MOPSO. J Intell Fuzzy Syst 2017;32(3):1753–73.
[64] Wiles J. Photovoltaic power systems and the national electrical code: suggested practices. Sandia National Lab. (SNL-NM), Albuquerque, NM (United States); 2001.
[65] Amrollahi MH, Bathaee SMT. Techno-economic optimization of hybrid photovoltaic/wind generation together with energy storage system in a stand-alone micro-grid subjected to demand response. Appl Energy 2017;202:66–77.
[66] Zia MF, Elbouchikhi E, Benbouzid M. Optimal operational planning of scalable DC microgrid with demand response, islanding, and battery degradation cost considerations. Appl Energy 2019;237:695–707.
[67] Bhamidi L, Sivasubramani S. Optimal Planning and Operational Strategy of a Residential Microgrid With Demand Side Management. IEEE Syst J 2020;14(2):2624–32.
[68] Qin Z, Li W, Xiong X. Incorporating multiple correlations among wind speeds, photovoltaic powers and bus loads in composite system reliability evaluation. Appl Energy 2013;110:285–94.
[69] Jeffreys H. The theory of probability. OUP Oxford 1998.
[70] Lu N, Diao R, Hafen RP, Samaan N, Makarov Yv. A comparison of forecast error generators for modeling wind and load uncertainty. In: 2013 IEEE Power & Energy Society General Meeting; 2013. p. 1–5.
[71] Mohseni S, Brent AC. Quantifying the effects of forecast uncertainty on the role of different battery technologies in grid-connected solar photovoltaic/wind/micro-hydro micro-grids: An optimal planning study. J Energy Storage 2022;51:104412.
[72] Ripley BD. Stochastic simulation, vol. 316. John Wiley & Sons; 2009.
[73] Karuppiah R, Martín M, Grossmann IE. A simple heuristic for reducing the number of scenarios in two-stage stochastic programming. Comput Chem Eng 2010;34(8):1246–55.
[74] Trading Economics, New Zealand – Real Interest Rate. [Online], Available https://tradingeconomics.com/new-zealand/real-interest-rate-percent-wb-data.html.
[75] Senwei. SWT-50 kW wind turbine; 2022. [Online]. Available: https://www.windpowercn.com/products/11.html.
[76] JASolar. Half Cut PERC 330 W PV panel; 2018. [Online]. Available: https://www.jasolar.com/uploadfile/2018/1215/20181215013846731.pdf.
[77] Tesla. 14-kWh Tesla Powerwall battery bank; 2019. [Online]. Available: https://www.tesla.com/sites/default/files/pdfs/powerwall/Powerwall%202_AC_Datasheet_en_AU.pdf.
[78] Schaefer Power. 50-kW rated Red Prime AC/DC converter; 2022. [Online]. Available https://www.schaeferpower.com/wp-content/uploads/2015/12/Schaefer_Full_Catalog.pdf.
[79] Samlex, 2022. 360 W SAMLEX IDC DC/DC converter. [Online]. Available: https://samlexamerica.com/products/fully-isolated-converter-idc-360c-12.
[80] Eaton. 21-kW Eaton DG IP21 DC/AC inverter; 2017. [Online]. Available: https://www.eaton.com/content/dam/eaton/support/catalog/eaton-dc%20-product-catalogue-new-en-gb-anz.pdf.
[81] SolarEdge. SolarEdge EV charger; 2022. [Online]. Available: https://www.solaredge.com/products/solaredge-ev-charger#.
[82] Kennedy J, Eberhart R. Particle swarm optimization. In: Proceedings of ICNN'95-international conference on neural networks; 1995, vol. 4, pp. 1942-1948.
[83] Mirjalili S. Moth-flame optimization algorithm: A novel nature-inspired heuristic paradigm. Knowl Based Syst 2015;89:228–49.
[84] Naruei I, Keynia F. Wild horse optimizer: a new meta-heuristic algorithm for solving engineering optimization problems. Eng Comput 2022;38(4):3025–56.
[85] Zhao W, Wang L, Mirjalili S. Artificial hummingbird algorithm: A new bio-inspired optimizer with its engineering applications. Comput Methods Appl Mech Eng 2022;388:114194.
[86] Abdollahzadeh B, Gharehchopogh FS, Mirjalili S. Artificial gorilla troops optimizer: A new nature-inspired metaheuristic algorithm for global optimization problems. Int J Intell Syst 2021;36(10):5887–958.
[87] Faramarzi A, Heidarinejad M, Mirjalili S, Gandomi AH. Marine Predators Algorithm: A nature-inspired metaheuristic. Expert Syst Appl 2020;152:113377.
[88] Faramarzi A, Heidarinejad M, Stephens B, Mirjalili S. Equilibrium optimizer: A novel optimization algorithm. Knowl Based Syst 2020;191:105190.
[89] MATLAB, The MathWorks Inc, Natick, MA; 2022. R2022a.
[90] Kaabeche A, Ibtiouen R. Techno-economic optimization of hybrid photovoltaic/wind/diesel/battery generation in a stand-alone power system. Sol Energy 2014;103:171–82.
[91] Ramli MAM, Bouchekara HREH, Alghamdi AS. Optimal sizing of PV/wind/diesel hybrid microgrid system using multi-objective self-adaptive differential evolution algorithm. Renew Energy 2018;121:400–11.
[92] Ogunjuyigbe ASO, Ayodele TR, Akinola OA. Optimal allocation and sizing of PV/Wind/Split-diesel/Battery hybrid energy system for minimizing life cycle cost, carbon emission and dump energy of remote residential building. Appl Energy 2016;171:153–71. https://doi.org/10.1016/j.apenergy.2016.03.051.
[93] Li B, Roche R, Paire D, Miraoui A. Sizing of a stand-alone microgrid considering electric power, cooling/heating, hydrogen loads and hydrogen storage degradation. Appl Energy Nov. 2017;205:1244–59.
[94] Darras C, et al. Sizing of photovoltaic system coupled with hydrogen/oxygen storage based on the ORIENTE model. Int J Hydrogen Energy 2010;35(8):3322–32.
[95] US Dollar to New Zealand Dollar Spot Exchange Rates for 2021. [Online], Available, https://www.exchangerates.org.uk/USD-NZD-spot-exchange-rates-history-2021.html.